# Energy Conversion Factors in Underwater Radiated Sound from Marine Piling

## Review of the method and recommendations

October 2023

Scottish Government
Riaghaltas na h-Alba

Suggested citation:

Wood, M.A., M.A. Ainslie, and R.D.J. Burns. 2023. Energy Conversion Factors in Underwater Radiated Sound from Marine Piling: Review of the method and recommendations. Document 03008, Version 1.2. Technical report by JASCO Applied Sciences for Marine Scotland.

# Contents

# Figures

## Tables

# Executive Summary

This project was commissioned by Marine Scotland, with the aim to improve the understanding of the Energy Conversion Factor (ECF) method, and to make recommendations regarding the modelling approaches for impact piling as used in environmental impact assessments (EIA) in Scottish Waters.

It is necessary to distinguish the genuine ECF, which is the ratio of the total sound energy in the water column to the hammer input energy, from what is termed the point-source equivalent ECF. The point-source equivalent ECF method involves calculating a broadband source level for a pile based only on the hammer strike energy and a value for the conversion factor. Sound source energy is then distributed over frequency bands based on a typical piling spectrum, and propagation losses calculated such that the sound field can be generated.

The key finding from this work is that, while the standard use of ECFs for piling is entirely valid, the process of generating a source level and propagating using point source models as used by the point-source equivalent ECF method reproduces the sound field from piling poorly. While there are concerns raised about the selection of a suitable value of ECF, greater errors are likely to arise in the choice of propagation models.

Values of the ECF in research show a range from 0.17 % to 1.56 % (9.6 dB). In EIAs where the method is used, a value of 0.5 % or 1.0 % has been arbitrarily chosen. Whilst these values sit well within the range of expected ECF values, there has been no regard for aspects of the operations that would affect this value. The difference between using an ECF of 0.5 % and 1.56 % is 4.9 dB, indicating that equivalent levels may be underpredicted by that much. There are few reported values of the ECF from measurements and modelling, and those that do exist are in shallow waters. Where point-source equivalent ECFs have been estimated by back-propagated point source model results, a much wider range of values has been generated (up to 13%).

In terms of sound propagation, the nature of a point source is to transition from a spherical spreading regime ($\propto 20\log_{10}(r)$) to a cylindrical spreading regime ($\propto 10\log_{10}(r)$) to a mode-stripping (or intermediate) regime ($\propto 15\log_{10}(r)$). The sound field from impact piling, however, features a Mach cone wavefront for which the propagation within the first few kilometres is described by the damped cylindrical model (DCS) ($\propto 10\log_{10}(r) + \alpha r$). These differences result in very different rates of energy loss and can lead to over or underestimates in the region of 10 dB within 5 km of the pile.

Combining the effect of predicting the source level using a point-source equivalent ECF of 0.5 % and using point-source propagation for one presented example yielded underestimates of the per-pulse sound exposure levels between 100 and 1000 m from the pile of between 9.5 and 12.1 dB. Using the point-source equivalent ECF method for a benchmark case scenario similarly showed underestimates between 6.3 and 10.2 dB for receivers at 250, 750, and 1500 m from the pile.

The recommendation is that the point-source equivalent ECF method, i.e., the combination of source level prediction and point-source propagation modelling, should not be accepted in EIAs due to the evident errors in its predictions. Whilst there may be potential for ECFs to be used in the prediction of noise from offshore piling, it would require a significant amount of development due to the many factors controlling the ECF and few studies that report it. Additionally, such an approach would need the source output to be coupled to an appropriate model. Sound propagation calculations using a point source model to represent a pile, as used in the reviewed reports, can result in substantial errors with examples showing deviations of around 10 dB within 5 km Alternatives are suggested depending on the availability of data and the level of detail required. In cases where measurements are available for the operation, sound field estimates can be reasonably well retrospectively calculated using the DCS model. In cases where measurements for similar operations exist there has been some success in applying scaling laws to account for changes in input parameters to generate sound field predictions. Additionally, sensitivity studies have been performed for operations in the US to generate recommendations as to when existing model data can be reapplied to a new prediction or if new modelling is required. In cases where some aspect of the pile, the hammer, or the environment of the scenario to predict is sufficiently different from those available in previous works numerical modelling using models that are designed specifically for piling is recommended. Furthermore, if complex environments, underwater piling, raked piles, or mitigation techniques such as bubble curtains are present, numerical modelling is recommended.

# List of Abbreviations

| | |
|---|---|
| DCS | damped cylindrical spreading |
| ECF | energy conversion factor |
| EIA | environmental impact assessment |
| ESL | energy source level |
| FD | finite-difference |
| ISO | International Organization for Standardization |
| PDSM | Pile-driving Source Model |
| PE | parabolic equation |
| PTS | permanent threshold shift |
| RAM | Range-dependent Acoustic Model |
| RD | range dependent |
| RI | range independent |
| SEL | sound exposure level |
| SSP | sound speed profile |

# 1. Introduction

Impact piling is a very common occurrence in marine construction projects, such as the installation of turbines for offshore wind farms. The process of impact piling has been shown to generate loud impulsive sounds that propagate into the marine environment. Due to the potential deleterious effects, it is necessary to produce predictions of the radiated sound field from piling operations for impact assessments. Noise modelling is commonly used to generate these sound levels given inputs from the hammer, the pile, and the environment. For most sources, this would typically involve separate calculation of a source function and the propagation loss to determine sound level fields emanating from the source. One method of calculating sound fields has been to predict point source sound levels representing the pile using the 'Energy Conversion Factor' (ECF).

The ECF represents the acoustic radiation efficiency of the hammer-pile system and is simply the ratio of the input hammer energy to the radiated sound energy. Using the ECF and a given hammer energy, one can estimate the total acoustic energy radiated into the water column, and consequently the sound exposure levels. Recorded ECFs in literature range from 0.17 % to 1.56 % and take into account every other energy loss mechanism in the piling strike. As such, it represents properties of the hammer, the pile, and the environment in terms of how much sound is radiated from the pile. Given that the range of ECFs span almost 10 dB, the selection of a suitable value will have a large effect on the sound field. It is not fully understood, however, exactly how one arrives at a suitable value of the ECF without prior numerical modelling.

One method for using the ECF has been to generate source levels directly to represent the piling. To separate this from standard uses of the ECF, we have termed this as point-source equivalent ECF throughout this report. The point-source equivalent ECF model provides the source levels of a point source pile which are propagated into the modelled domain using standard underwater acoustic point source propagation models. This method has been used in numerous Environmental Impact Assessments (EIA) to provide sound field predictions from impact piling.

This project was commissioned by Marine Scotland, with the aim to improve the understanding of the point-source equivalent ECF method, and to make recommendations regarding the modelling approaches for impact piling as used in EIAs in Scottish Waters. This report shows the results of the project findings and is structured as follows. Section 2 provides background on derived values of the ECF as applied to impact piling in literature, a review of the use of the point-source equivalent ECF that appear in EIAs and articles, and a brief overview of acoustic propagation models that are commonly used for impact piling. Section 3 shows the results of studies comparing the differences between line source acoustic models, designed for use with piling, and point source models, which includes the point-source equivalent ECF method studied here. Examples are shown for simple

geometric models and high-resolution numerical models to show how to different methods of propagation differ and the implications of using the wrong model. Section 4 provides an overview of possible methods for predicting sound levels from piling. These include predictions based on existing measurements and full-scale numerical modelling. Finally, Section 5 provides a summary of the findings and recommendations for future projects.

# 2. Review of Current Practices

This section provides a review of the ECF as it has been used in certain acoustic modelling projects providing predictions of the radiated sound field from marine piling operations. The section is divided based on two distinct aspects of the modelling. First, we look at how the source is defined in these projects, and the shortcomings of current methods. Second, we pay closer attention to how the propagation of sound is modelled.

## 2.1. The Pile as a Sound Source

The most common general method for predicting underwater sound levels resulting from an audible process in the water is to start with a source level and calculate the propagation loss, i.e., attenuation of sound, between the source and the receiver. Consequently, based on this method, a reasonable prediction of the source level is required.

It must be made clear at this stage that in the case of impact piling there is no source level for reasons that are discussed later in this section; it would be technically incorrect to refer to it as such. In this context, however, the pile is reproduced as a point source somewhere in the water column.

It is also valuable to note that there is a distinction between ‘source level’ and ‘energy source level’, with full definitions provided in ISO 18405:2017. The source level is related to the mean-square sound pressure of a statistically stationary sound source, i.e., one that is providing constant continuous sound, and thus is independent of time. The energy source level is based on the time-integrated squared sound pressure, and thus is a measure of the total sound energy within a set time interval. Given the nature of the piling pulse, it is more appropriate to use the energy source level over the source level.

Use of the “acoustic energy conversion efficiency” to convert to the “source level energy” of a pile driving strike is described by Farcas et al. (2018) in the following extract:

> “The source level estimate for pile driving was calculated using an energy conversion model, whereby a proportion of the expected hammer energy is converted to acoustic energy:
>
> $$SL_E = 120 + 10\log_{10}\left(\frac{\beta E c_0 \rho}{4\pi}\right)$$
>
> where $E$ is the hammer energy in joules, $SL_E$ is the source level energy for a single strike at hammer energy $E$, $\beta$ is the acoustic energy conversion efficiency, $c_0$ is the speed of sound in seawater in $ms^{-1}$, and $\rho$ is the density of seawater in kg $m^{-3}$”

The source level (or energy source level) of an underwater sound source is defined in terms of its far-field sound pressure. From ISO 18405 (2017), the acoustic far field is the “spatial region in a uniform medium where the direct-path field amplitude, compensated for absorption loss, varies inversely with range”. In Section 2.1.1, we explain that the sound propagation from a driven pile does not fulfil the criterion for a far-field state as described above; as the driven pile has no far field it therefore has no source level (Ainslie et al. 2020). For other sound sources of potential interest, one can write a similar equation

$$L_{S,E} = K + 10\log_{10}\left(\frac{\frac{\beta E c_0 \rho_0}{4\pi}}{1\ \mu\mathrm{Pa^2 m^2 s}}\right)\mathrm{dB}\,. \tag{1}$$

Here, $c_0$ and $\rho_0$ are the sound speed and density of the medium, $E$ is the input energy to the source (for an airgun this could be the potential energy stored in the compressed air; for a sonar pulse it could be the electrical energy used to drive the transducer), and $\beta$ is the ECF.

As a pile driver does not have a source level, Equation 1 is not applicable. Nevertheless, it has been used (Cefas 2018a, Cefas 2018b, Farcas et al. 2018, Cefas 2019, Faulkner et al. 2021, Seiche Ltd 2022) to estimate the sound field radiated by a point source of the same energy as the pile driver. The frequency dependence of the source is then provided by using previously recorded spectra and applying a uniform offset in dB across all frequency bands to match the calculated energy source level. The approximations incurred by assuming the pile can be represented by a point source (with a far field) are addressed in Section 3.

Equation 1 provides a simple expression for the broadband energy source level, for which three of the four variables ($c_0$, $\rho_0$, and $E$) are typically readily available. Presuming temporarily that the equation was suitable for impact piling, the ECF would then represent every other aspect of the sound generating mechanisms within the impact. Consequently, it is possible that it would be a function of many other inputs including: hammer properties such as ram mass, and helmet/anvil properties; the pile properties such as diameter, length, and wall thickness; and the environmental properties including water depth, and the sediment make up. For a single value to be valid, it must be shown that it is relatively insensitive to changes in these input parameters.

It is useful to reiterate that the ECF is a value that does indeed exist for the pile as an acoustic source. The ‘source level’ of an impacted pile, however, does not exist. Consequently, any use of the ECF to generate a source level for a pile is fundamentally flawed. Similarly, calculations of the ECF using received sound levels back-propagated to a point source are equally invalid. To avoid ambiguity between genuine calculated results of the ECF, and the those incorrectly used, the latter has been termed the ‘point-source equivalent ECF’.

The following section provides insight into the origin of Equation 1. Section 2.1.2 follows on to review calculations of the ECF for impact piling, and Section 2.1.3 covers use of the point-source equivalent ECF for environmental impact assessments and other articles.

### 2.1.1. Derivation of the energy conversion factor expression

The energy conversion factor has its roots in an expression for source energy presented by de Jong and Ainslie (2008) in the conference paper "Underwater radiated noise due to the piling for the Q7 Offshore Wind Park", presented at "Acoustic 08 Paris". The energy conversion factor has since been defined as the ratio of the impact energy of the hammer to the acoustic source energy radiated into the water column. It is instructive to determine the origin of the expression. For this, we need to define a few terms, which are all based on ISO 18405 (2017).

Sound energy, $H$, is the integral of sound power, $W(t)$, integrated over time between $t_1$ and $t_2$, i.e.,

$$H = \int_{t_1}^{t_2} W(t)\mathrm{d}t \ . \tag{2}$$

Sound power is the surface integral of the component of sound intensity, $\boldsymbol{I}(x,t)$, normal to the integration surface, $S$ (ISO 18405: 3.1.3.14):

$$W(t) = \int I_{\mathrm{n}}(x,t)\mathrm{d}S \ , \tag{3}$$

such that

$$H = \iint_{t_1}^{t_2} I_{\mathrm{n}}(x,t)\mathrm{d}t\mathrm{d}S \ . \tag{4}$$

In the far field, the time-integrated squared sound pressure (equivalently, the sound exposure, $E_{p,T}$, ISO 18405: 3.1.3.5) is equal to the product of the characteristic acoustic impedance, $Z_{\mathrm{c}}$, of the medium (ISO 18405: 3.1.5.6) and the magnitude of the time-integrated sound intensity (ISO 18405: 3.1.3.10). Additionally, in spherically symmetrical space, we replace $x$ with $r$ where $r$ is the distance from the acoustic centre. This provides the relationship:

$$\int_{t_1}^{t_2} I_{\mathrm{n}}(x,t)\mathrm{d}t = \frac{1}{Z_{\mathrm{c}}}\int_{t_1}^{t_2} p^2(r,t)\mathrm{d}t = \frac{E_{p,T}(r)}{Z_{\mathrm{c}}} \ . \tag{5}$$

Furthermore, based on far-field assumptions, one can define the energy source factor, $F_{\mathrm{S},E}$, (ISO 80405 3.3.1.5) as

$$F_{\mathrm{S},E} = r^2 E_{p,T}(r) \ . \tag{6}$$

Noting that the source factor is independent of $r$, we can further write

$$H = \frac{F_{S,E}}{Z_c} \int \frac{1}{r^2} \mathrm{d}S \ . \tag{7}$$

Taking the surface integral over a sphere at distance $r$ from the acoustic centre provides a surface area of

$$S = 4\pi r^2 \ , \tag{8}$$

and the result of the integral in Equation 7 as

$$H = \frac{4\pi F_{S,E}}{Z_c} \ . \tag{9}$$

It is useful to note that the energy source factor can be written in terms of a sound exposure source level, $L_{S,E}$, (ISO 18405 3.3.2.2) given by

$$L_{S,E} = 10 \log_{10} \left( \frac{F_{S,E}}{F_{S,E,0}} \right) \mathrm{dB} \ , \tag{10}$$

where the reference value, $F_{S,E,0}$ is 1 μPa²m²s (i.e., $10^{-12}$ Pa²m²s). Consequently, it follows that

$$F_{S,E} = 10^{\frac{L_{S,E}}{10\ \mathrm{dB}}} F_{S,E,0} = 10^{\frac{L_{S,E}}{10\ \mathrm{dB}}} \times 10^{-12} \mathrm{Pa^2 m^2 s} = 10^{\frac{L_{S,E} - 120\ \mathrm{dB}}{10\ \mathrm{dB}}} \mathrm{Pa^2 m^2 s} \ . \tag{11}$$

Additionally, the characteristic acoustic impedance in terms of medium density, $\rho_0$, and the speed of sound, $c_0$, is

$$Z_c = \rho_0 c_0 \ . \tag{12}$$

Insertion of these into Equation 9 provides the quoted formula from the paper of

$$H = \frac{4\pi}{\rho_0 c_0} 10^{(L_{S,E} - 120\ \mathrm{dB})/(10\ \mathrm{dB})} \mathrm{Pa^2 m^2 s} \ . \tag{13}$$

In this derivation, there are two crucial assumptions regarding the nature of the sound propagation. Firstly, it is presumed that there exists some region far from the source where the direct-path field amplitude varies inversely with range. Secondly, it is required that the source exists in a single medium, i.e., with a uniform characteristic acoustic impedance surrounding the source. Both need to be satisfied for the source level to exist.

With regards to these two requirements in the context of impact piling, the topic has been directly addressed in the literature. To directly quote from Ainslie et al. (2020):

> "An impact-driven pile does not have a source level for two reasons. First, source level (ISO 2017) is defined in terms of the sound radiated by a source into its far field, where the propagation is spherical. For an impact-driven pile, the extent of the source throughout the entire water column from seafloor to sea surface results in cylindrical spreading from the pile wall (Dahl et al. 2012, Zampolli et al. 2013). Thus there exists no region of spherical spreading, and

> therefore no far field. Second, the same definition of source level invokes the concept of “a hypothetical infinite uniform lossless medium of the same density and sound speed as the real medium at the location of the source,” and therefore a source level is only defined if the source in question is in contact with a single uniform medium. The pile is in contact with a layered medium comprising water and sediment, with at least two different impedances, and therefore also does not meet this second criterion for the definition (i.e., existence) of a source level."

This distinction was noted by Zampolli et al. (2013), where it was written that “…the pile should not be represented by a point source, but rather by a conical Mach wave”. The formulation that followed provides an expression for the acoustic energy in the water column as a function of range that considers the angled wavefront of the Mach wave between the water surface and the seafloor. This derivation was validated against the numerical model results in the paper and forms the basis of the damped cylindrical spreading model (Lippert et al. 2018).

In the case of the impacted pile, as stated, there is no far field and no source level. The total sound energy of the piling pulse is dependent on the location of the surface over which sound power is integrated regardless of whether the pile is slightly embedded in the seabed or driven almost entirely in. As the apparent sound energy varies with the integrating surface, rather than the constant value achieved with the point source case, Use of Equation 13 in the context of piling leads to errors that are quantified in this report.

### 2.1.2. Values for the energy conversion factor

As stated earlier, one significant variable in the description of the energy source level from Equation 1 is $\beta$, i.e., the ECF. As previously stated, it is defined as

$$\beta = \frac{H}{E}, \tag{14}$$

i.e., the ratio of the radiated sound energy in the water to the input hammer energy. The ECF is significant in that it represents many aspects of the piling situation and directly controls the acoustic output of the system. It is unclear exactly how the ECF is affected by the system inputs; however, attempts have been made to calculate the relative amount of hammer energy that is converted into acoustic energy based on both measurements and modelling.

There are only few reported instances of an energy conversion ratio in literature. The methods of calculation vary from considering the pile to be a point source and back-propagating from measurements, to calculating it directly from full finite-element models of the pile. As stated, and will be shown in more detail in Section 3, point source models are now known to be inappropriate for the back-propagation; they were, however, considered best available science 12 years ago and so were employed for pile modelling.

There is no direct way to measure the energy radiated from the pile. For field studies it is necessary to approximate the energy typically achieved using measurements of SEL close to the pile. From Equations 4 and 5 we can show that the total sound energy in the water column, $H$, is related to the sound exposure, $E_{p,T}(r)$ as

$$H = \frac{1}{Z_C} \int E_{p,T}(r) \mathrm{d}S \tag{15}$$

where the surface integral is taken over a cylinder spanning the water column. If we can assume radial symmetry and a depth-averaged value of sound exposure, $\bar{E}_{p,T}(r)$, we can rewrite this as

$$H = \frac{A(r)\bar{E}_{p,T}(r)}{Z_C} \tag{16}$$

where $A = 2\pi r D$ (i.e., the surface area of the cylinder excluding ends) and $D$ is the water depth. The energy conversion factor, $\beta$, is then provided by Equation 14.

In the report, “The measurement of the underwater radiated noise from marine piling including characterisation of a “soft-start” period”, Robinson et al. (2007) shows results for the driving of a 2 m diameter, 65 m long pile using hammer energies from 80 kJ to 800 kJ into chalk with local water depths ranging from 8 to 15 m. The observation of the correlation between SEL at 57 m from the pile and input hammer was made with results shown in Figure 1. Here, they calculate the gradient of the line and state that “about 0.3 % of the hammer energy is converted to sound”.

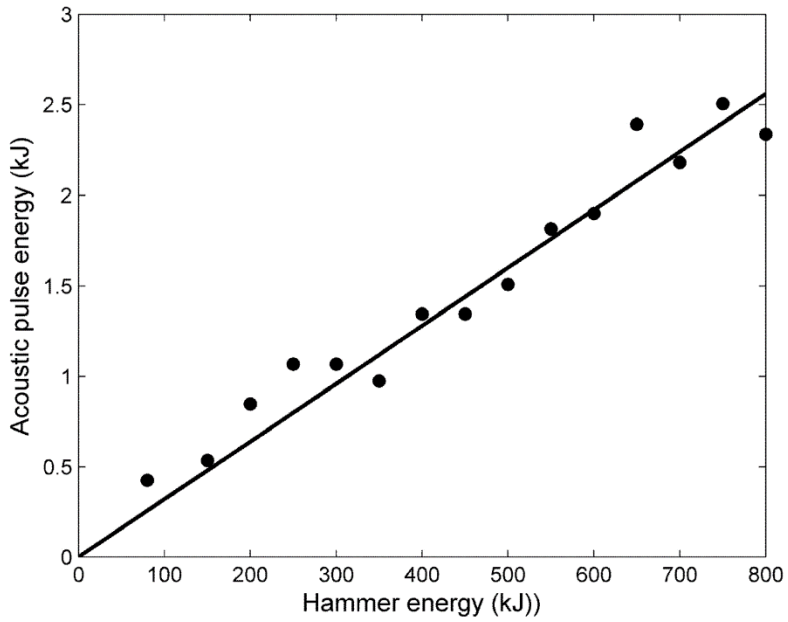


Figure 1. Back-propagated acoustic pulse energy against input hammer energy for measurements of offshore piling reproduced from Robinson et al. (2007). The gradient of the best-fit line has a gradient of 0.32 %.

In a *tour de force*, Reinhall and Dahl (2011) coined the term 'Mach' cone, which describes the shape of the wavefront propagating from the pile; as the stress wave travels down the length of the pile, the local compressions results in a wall expansion at that point, creating an increase in pressure at the pile wall that moves down the pile at the speed of sound in the pile, thus resulting in conical wavefronts at a single angle (Figure 2). This was revolutionary as, before this, it was common to model the impacted pile as a point source; this paper showed that the point source assumption for piles was fundamentally wrong.

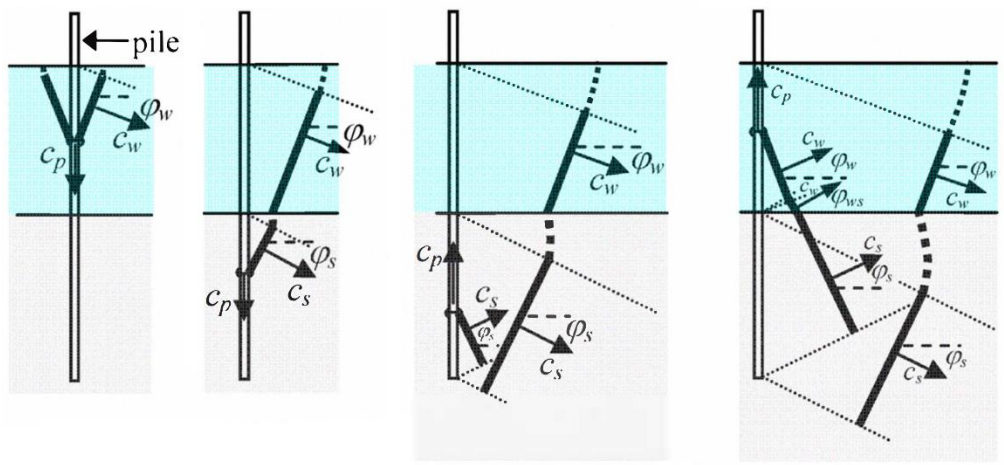


Figure 2. Time snapshots of the stress wave down the pile and the radiated acoustic wave in the characteristic conical wavefront (Mach cone). Reproduced from Reinhall and Dahl (2011).

In their report "Beam forming of the underwater sound field from impact pile driving", Dahl and Reinhall (2013) presented measurements made in Puget Sound of a 0.762 m diameter pile and 32 m long, driven into the sediment. Measurements were made close to the pile using a vertical line array of hydrophones. Given a hammer energy of 180 kJ, and estimated sound energy of 2400 ± 400 kJ from the complete set of line source measurements, the ECF was calculated to be between 1.11 % and 1.56 %.

Zampolli et al. (2013) used highly detailed finite-element modelling of an impacted pile alongside an experimental set up in Kinderdijk. The pile in this case was a capped pile, 32.4 m long, with a diameter of 0.914 m, driven into medium sand. From the validated model results they calculated the energy radiated horizontally by the pile into the water to be 1.164 kJ, and the energy transferred from the hammer to the anvil to be 54.6 kJ resulting in a ratio of 2.13 %. If one considers the input hammer energy of 87 kJ rather than just that transferred to the pile, this provides an ECF of 1.33 %.

From the finite element model, Zampolli et al generated a figure of the horizontal component of the energy in the water and sediment both together and separately against a geometric spreading curve. The geometric spreading curve here is based

on the description of the acoustic field in terms of the conical Mach wave rather than from a point source. The match between the finite-element model and the geometric spreading curve showed the viability of this approach.

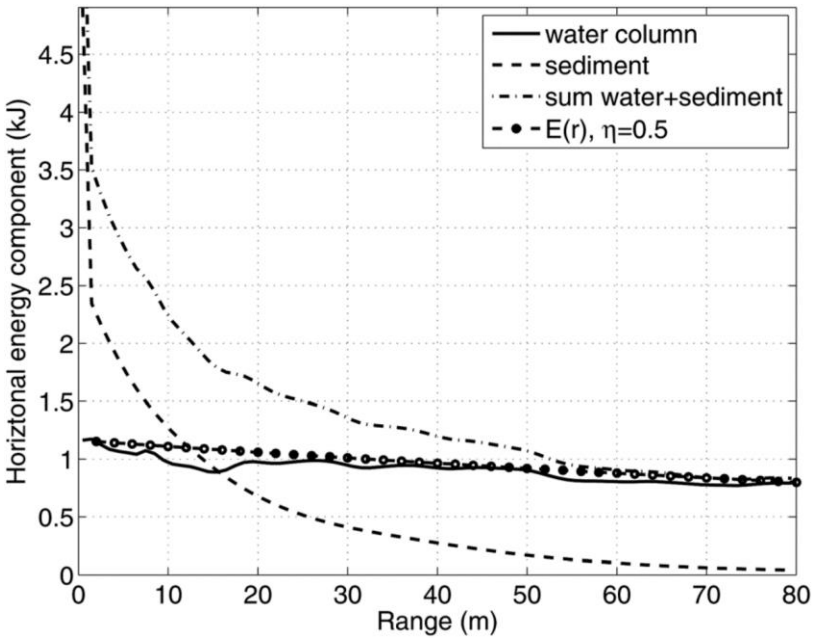


Figure 3. Plots of the horizontal component of the energy from the finite-element model by Zampolli et al. (2013) showing energy in the water column, the sediment, the water and sediment combined, and from a geometric spreading model ("E(r), η=0.5") derived from consideration of Mach cone propagation.

The ratio of energy from the hammer to the sound energy is mentioned in an article by Dahl, de Jong, and Popper called "The Underwater Sound Field from Impact Pile Driving and Its Potential Effects on Marine Life" (2015). The article references the sources mentioned above to suggest that "~0.5 % of this hammer energy goes into acoustic energy that ultimately gets into the water column". However, no additional results are presented, and so this value is presumed to be a ballpark figure given the range of calculated values from the cited references (ratios of 0.32 %, 1.11 % to 1.56 %, and 1.33 %).

A further study into the impact pile driving sound field, with a focus on energy streamlines is one presented by Dahl and Dall'Osto (2017). The study relates to a 23.5 m long pile, with a diameter of 0.762 m, driven using an impact energy of 198 kJ. The water depth was 7.5 m, and the pile was driven to a depth of 12 m using an input hammer energy of 198 kJ. The radiated sound field was modelled using Range-dependent Acoustic Model (RAM), representing the pile as many point sources with appropriate phase delays such as to recreate the Mach cone acoustic wavefront in the water. The total energy in the water column was calculated at 60 m (water depth of 7.5 m) and 120 m (water depth of 12.5 m) from the pile using the model results. At 60 m, the total energy in the water column was 260 J, and at 120 m it was 235 J; these correspond to 0.12-0.13 % of the input energy. If one presumes a

similar rate of energy loss as seen for the Kinderdijk pile in Figure 3, given the similarity in water depths, the total acoustic energy entering the water column at the pile wall is approximately 345 kJ, providing an ECF of 0.17 %.

To summarise, the results here provide values of ECF calculated from the time-integrated sound intensity integrated over a cylinder close to the pile to provide the total sound energy in the water column. Where measurements are used, the time-integrated sound intensity is estimated using results for the sound exposure level using Equation 5. The range of ECFs calculated here are between 0.17% and 1.56%; this equates to a range of 9.6 dB.

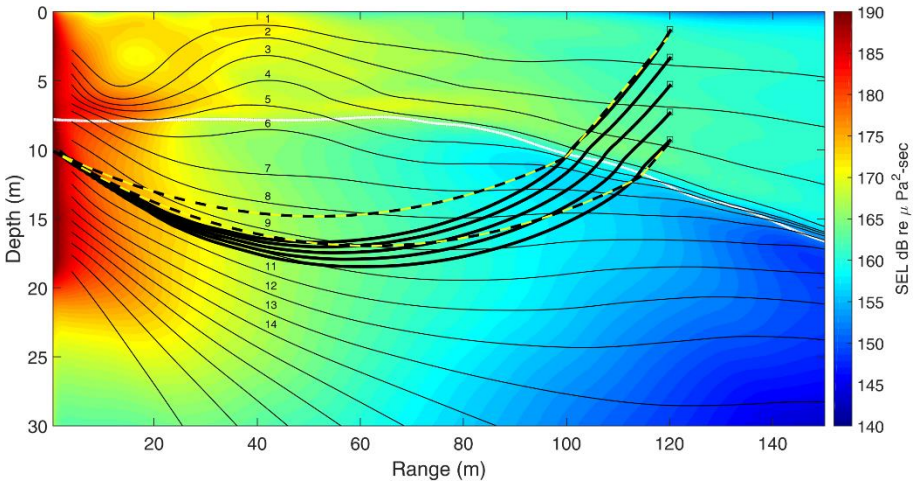


Figure 4. SEL sound field reproduced from Dahl and Dall'Osto (2017). Although not discussed here, the thin black lines indicate the energy streamlines tangent to time-integrated intensity (i.e., over entire pulse), thick black lines indicate instantaneous energy path lines launched from five locations corresponding to the measurement positions, black and yellow lines indicate the paths of two ray launched from 10 m depth.

### 2.1.3. Use of the point-source equivalent ECF

Despite the approximations implied by treating a pile driver as a point source, forward predictions of sound fields using the point-source equivalent ECF method have appeared in reports supporting EIAs for pile driving operations. Additionally, the method has been used in other articles in a similar regard. This section provides a brief overview of its use in these works, and other points of note regarding their application. A summary of the reviewed EIAs is provided in Table 1.

Table 1. Reviewed works employing the ECF in forward predictions.

| Report | Year | ECF | Notes |
|---|---|---|---|
| Beatrice Offshore Windfarm Ltd (BOWL): Piling strategy | 2015 | 1.0 % | $15\log_{10}(r)$ propagation |
| Seagreen Offshore Wind Farm | 2018 | 0.5 % / 1.0 % | Additional work performed using 1.0 % requested by Marine Scotland Licensing and Operations Team |
| Inch Cape Offshore Wind Farm | 2018 | 0.5 % / 1.0 % | Additional work performed using 1.0 % requested by Scottish Natural Heritage |
| Moray West Offshore Wind Farm | 2018 | 0.5 % / 1.0 % | Recalculated at 1 % as supplement to EIA |
| Moray East Offshore Wind Farm | 2019 | 0.5 % / 1.0 % | Recalculated at 1 % as supplement to EIA |
| Sizewell C Project | 2021 | 0.5 % / 1.0 % | 1.0 % only for pile diameter >2 m |
| Berwick Bank Wind Farm | 2022 | 4.0 % to 0.5 % | 4.0 % reducing to 0.5 % and others for context |

The earliest found appearance of the method was found in the Piling Strategy report for Beatrice Offshore Wind Farm (2015). The acoustic modelling was for pin piles with a diameter of 2.2 m being driven by a hammer with an input energy of 300 kJ. The summary of the acoustic modelling in the section 'identification of impact zones' refers to using a point-source equivalent ECF of 1.0 %, which for a 300 kJ hammer provides a per-pulse energy source level (ESL) of 205.6 dB re 1 μPa²m²s. The propagation loss was erroneously assumed to be "$15\log_{10}(r)$" with the only reasoning being that the operations were in shallow waters. While a $15\log_{10}(r)$ dependence is possible in shallow water, there is always an additional additive constant (Equation 21).

The next uses of the point-source equivalent ECF in reviewed works were for Seagreen (Farcas et al. 2018) and Inch Cape (Cefas 2018b) offshore wind farms. Seagreen featured 2 m diameter pin piles and 10 m diameter monopiles driven with hammer energies of up to 3000 kJ, while Inch Cape had 2.5 m diameter pin piles and 12 m diameter monopiles using respective hammer energies of up to 2400 kJ and 5000 kJ. The source model for each was the same as for Beatrice; the propagation, however, was modelled using an implementation of RAM, which is a well-established underwater acoustic propagation model and described more in Section 2.2.2. Propagation was calculated at 10 discrete frequencies per "1/3-octave-band" (broadly equivalent to decidecade bands) and summed to generate the full sound field; it is not clear, however, what the maximum frequency modelled was, which would be an important aspect in the consideration of frequency-weighted sound levels. The depth-averaged sound levels were taken to generate the noise maps.

It's notable that for these two works, the initial modelling work was carried out using an point-source equivalent ECF of 0.5 % but was revisited using a value of 1.0 % after scrutiny from the regulator (Cefas 2018c, Cefas 2018d). The effect of changing the point-source equivalent ECF from 0.5 % to 1.0 % is equivalent to doubling the hammer energy or adding 3 dB to the energy source level (and consequently to all received levels). Results in these reports are typically shown as the distances to the points where the sound level drops below a given threshold. Whilst the change of point-source equivalent ECF from 0.5 % to 1.0 % resulted in no or modest increases in some scenarios, there are extreme examples of the modelling results where PTS impact ranges for minke whales went from <50 m for the value of 0.5 % to >10 km for 1.0 % (Table 1.6, Cefas 2018d). Whilst it seems unlikely that a 3 dB increase in sound levels would result in such a change, in this example it resulted in an impact significance change from 'Negligible' to 'Minor' (Table 1.9, Cefas 2018d).

Further works from this point onwards, used 0.5 % point-source equivalent ECF as a default value. The justification for this value is based on the results highlighted in Section 2.1.2, with particular attention drawn to the comment in Dahl, de Jong and Popper (2015). Moray West had modelling for pin piles driven with a maximum energy of 3000 kJ, and monopiles with 5000 kJ (Cefas 2018a). Moray East windfarm had modelling for pin piles of a diameter of 2.5 m driven with a maximum hammer energy of 2250 kJ (Cefas 2019). Both projects used point-source equivalent ECF values of 0.5 %, and the same methods as for the previous projects. In a more recent study, for piling as part of the Sizewell C Project, a point-source equivalent ECF of 0.5 % was used for smaller diameter piles (1.0 m) whilst 1.0 % was used for the larger diameter piles (2.5 m) as a 'precautionary' approach (Faulkner et al. 2021). There were no details, however, as to the propagation model employed.

The increased regulatory scrutiny applied to the choice of the point-source equivalent ECF led the recent EIA for Berwick Bank (Seiche Ltd, 2022), to include further investigatory studies. The Berwick Bank report presents sound fields for numerous activities associated with the construction through to decommissioning of the wind farm. One aspect of the assessment was for impact driven piles for jacket foundations. These anchor piles had a diameter of 5.5 m with maximum (maximum hammer energy of 4000 kJ) and realistic (maximum hammer energy of 3000 kJ) scenarios defined. Additionally, these pin piles are driven such that only a small portion of the pile remains above the seabed rather than the monopile construction consider thus far.

Because of the uncertainty around an appropriate choice of point-source equivalent ECF the authors provided results considering:

- a constant conversion factor of 1 %;
- a reducing conversion factor from 10 % to 1 % (based on Thompson et al. (2020)); and
- a reducing conversion factor from 4 % to 0.5 % (based on Lippert et al. (2017)).

Final results are presented for the reducing conversion factor from 4 % to 0.5 % given the ‘best balance of realism and precaution’. It is noted, however, that Lippert et al. (2017) do not provide direct calculations of the ECF, nor reference it in the paper. What is presented by Lippert et al., however, is the measured SEL normalised to a hammer energy of 2000 kJ at 750 m from the pile as function of penetration depth. One notable outcome is the observation that for the period where the pile was entirely below the water line, the SEL reduced by 2.5 dB per 50 % reduction of the remaining pile length in the water column.

It is stated that the conversion factors have been derived following further analysis of the Lippert data; although no details are provided as to the methods applied, it is likely that the same propagation model used to generate sound fields was used to back-propagate the Lippert et al. results to generate a point source level, from which a point-source equivalent ECF can be calculated using Equations 13 and 14 yielding values between 0.5 % and 2.0 %. Further adjustments were made to the conversion factor based on the pile length exposed to the water, increasing the upper value to 3.5 %; this is based on the assumption that the energy radiated is approximately proportional to the wetted portion of the pile.

The propagation model used in the Berwick Bank EIA departs from the PE model approach. Instead, an energy flux model derived by Weston (1976) is used. Its use in this context is described further in Section 2.2.3.

As stated, the point-source equivalent ECF has been used in articles outside of environmental impact assessments. The point-source equivalent ECF method (using a value of 0.5 %) was also used for forward predictions in an article by Graham et al. (2019). In the supplementary material of the article, the propagation model described is as before with the inclusion of a separate high-frequency model based on a point-source energy-flux model for 1.25 kHz and higher. The modelling results were compared against measurements at 2.0, 7.6, and 10.2 km. For broadband sound levels, it was found that per-pulse error in the predictions were 6.6, 2.0, and 0.8 dB re 1 μPa²s respectively.

In the study “Balancing risks of injury and disturbance to marine mammals when pile driving at offshore wind farms”, Thompson et al. (2020) provide analyses of piling operations involving four 35 to 45 m long piles, each with a diameter of 2.2 m driven by a hammer with energies ranging from 266 kJ to between 744 kJ and 1735 kJ. Sound level predictions were made for four piles using the point-source equivalent ECF method for receivers between 0.8 and 3.8 km from the piling operation at 2 m above the seabed. It was found that sound levels reduced for increased penetration depths given the same hammer energy input and that low-energy-low-penetration impacts resulted in greater sound levels than high-energy-high-penetration impacts. Consequently, the point-source equivalent ECF model, which generates “source levels” using only the hammer energy and a fixed value of $\beta$, provided a poor fit to the measured results (Figure 5).

Of note, is that the paper also provides calculations of what the point-source equivalent ECF ‘should’ have been to generate the observed received levels. Although the exact process is not documented it appears that the propagation loss between the idealised point source and the receiver has been calculated to determine a source level and consequently used to determine a value for $\beta$ throughout the piling sequence (Figure 6). Calculated values are between 13.2 % at the start of piling and 0.5 % towards the end. The calculated values at the start of the sequence are an order of magnitude higher than those obtained by other researchers, although the method by which the values are derived is unclear.

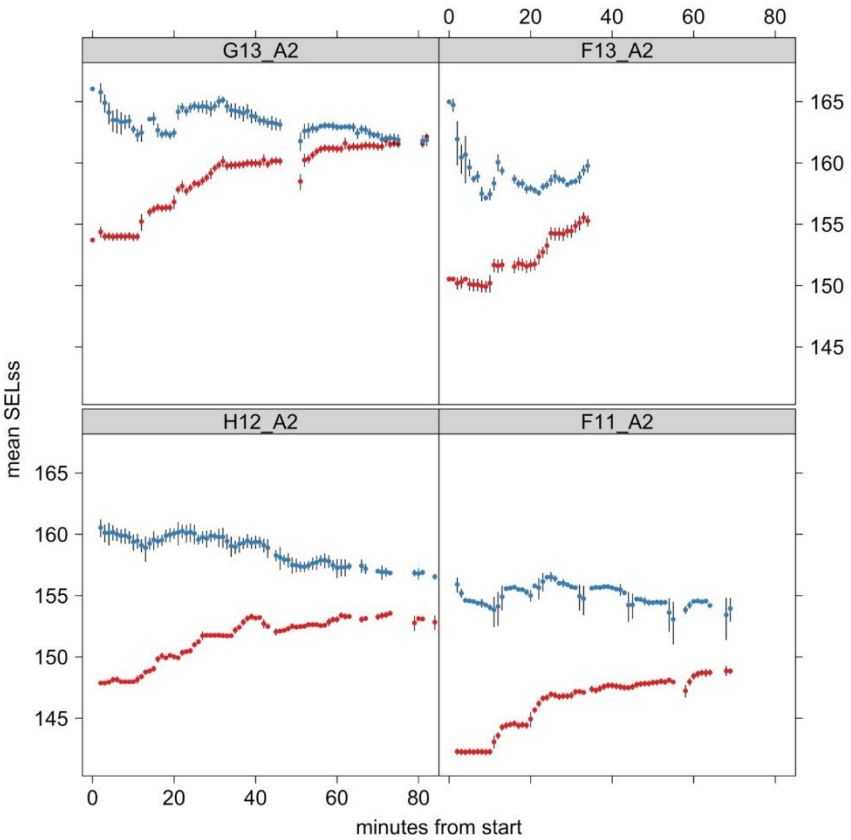


Figure 5. Modelled (red) versus measured (blue) per-pulse SEL for four piles between 0.8 km and 3.8 km from the piling operations reproduced from Thompson et al (2020). Modelling was carried out using the ECF method for the source function ($\beta$ = 0.5), and a point source propagation assumption in RAM and an energy flux model.

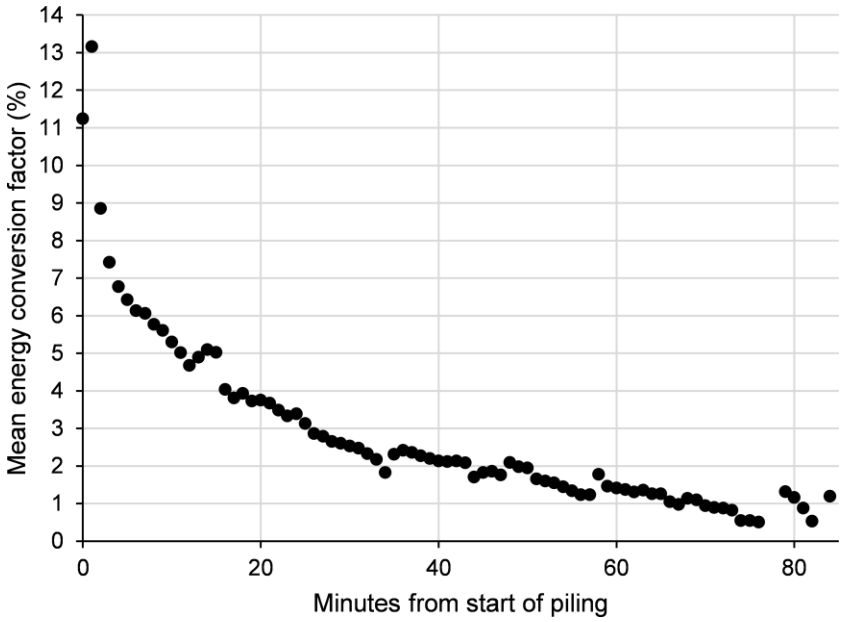


Figure 6. Point-source equivalent ECF calculated over the course of the piling sequence from back-propagated hydrophone measurements from Thompson et al (2020). The calculated value is between 0.5 % and 13.2 %.

It is noted that there have been no formalised methods for calculating the point-source equivalent ECF. It is clear, though, that the calculation is different from those discussed in Section 2.1.2. While it is fair to say that the amount of energy converted to acoustic energy is of the order of 1 % in many cases, there appear to be a wide range of results even for a single pile operation, where many elements likely to affect the point-source equivalent ECF (i.e., hammer parameters, pile parameters, and environment) are kept constant. The implication is that, even if using Equation 1 to calculate a source level were appropriate, it is currently unknown how to accurately generate a suitable value of point-source equivalent ECF.

As shown in Table 1, the value for point-source equivalent ECF in almost all cases has been either 0.5 % or 1.0 % with 1.0 % being considered a conservative value. The sound field differences between using 0.5 % and 1.0 %, however, can be very large indeed. Additionally, as shown in the previous section, there are many examples of where the calculated point-source equivalent ECF deviates from this substantially, often by an order of magnitude. The conclusion is that using a default point-source equivalent ECF value for all piling, is unlikely to provide robust sound field results.

No mention has been made regarding usage of the point-source equivalent ECF method in terms of predicting peak sound pressure levels. The approach adopted in these works has been to use empirical linear equations that relate the peak sound pressure level to the sound exposure level by Lippert et al. (2015). The use of these correlation equations is not under scrutiny and so are not reviewed here; however, they have been shown to provide very reasonable results and no concern is raised on the use of these equations where calculations of the SEL is reliable.

## 2.2. Sound Propagation Models

Following a description of the sound source, it is then necessary to characterise how the sound propagates through the environment. This section provides a very brief introduction to the more common model types that are used for underwater sound propagation. Additionally, further information is provided on RAM (an implementation of the parabolic equation model type), and energy flux models, both of which have been used in the propagation of sound from piling, including those covered in the modelling in Table 1.

### 2.2.1. Propagation model types

The propagation of sound, when considering standard linear acoustics, is fundamentally governed by what is known in physics as the wave equation. By solving the wave equation, given certain specified boundary conditions, one can characterise the sound field at all places and at all times. The equation relates the spatial variation of an acoustic parameter, typically sound pressure, to temporal variations in that same parameter. In its standard form, the equation is difficult to solve for general cases. There are techniques, however, that make the process easier. Principally, if one assumes the sound to be at only a single frequency, the time element can be removed from the wave equation. Doing this provides a simpler function known as the Helmholtz equation that describes sound propagation at a specific frequency. The Helmholtz equation is more readily solved, and typically models would calculate the sound field for each modelled frequency separately then sum them to generate the result for all frequencies.

Acoustic models generally differ in how they solve the Helmholtz equation. These can include, but are not limited to, the following:

- Parabolic equation (PE) models,
- Ray- or beam-tracing models,
- Wavenumber integration models,
- Normal mode models,
- Energy-flux models.

A full discussion of how the models are derived is beyond the scope of this work, but detailed descriptions can be found in literature such as Jensen et al. (2011). Each model type has its strengths and weaknesses, and it should be noted that no single model is the best across all situations (Wang et al. 2014). Table 2 shows the list of model types and their applicability to different acoustic problems from Etter (2012) with additions.

The piling pulse typically has a spectrum with a peak between 100-150 Hz; consequently, a model capable of handling lower frequencies is better suited than a high-frequency model. Given the environments where one finds wind farm

installations, one typically requires a model that is effective in shallow water. In the context of piling, where the principal frequency has wavelengths of between 10 and 15 m, shallow water would correspond to water depths associated with most of the continental shelf (up to approximately 200 m). Finally, it is often desirable to include bathymetric features, particularly for longer range propagation; thus, range-dependent models (i.e., ones that can handle changes in the water depth with a change in distance) are better suited. Based on Table 2, models based on the parabolic equation are most likely to yield useful results in these situations. For cases where there is little change in bathymetry, however, normal mode, wavenumber integration, and energy flux methods are very applicable.

Table 2. Domains of applicability of underwater acoustics propagation models reproduced from Etter (2012) with additions. Low frequency is <500 Hz, high frequency is >500 Hz; RI is range independent, RD is range dependent.

| Model type | Application | | | | | | | |
|---|---|---|---|---|---|---|---|---|
| | Shallow water | | | | Deep water | | | |
| | Low frequency | | High frequency | | Low frequency | | High frequency | |
| | RI | RD | RI | RD | RI | RD | RI | RD |
| Ray tracing | | | ◑ | ● | ◑ | ◑ | ● | ● |
| Parabolic equation | ◑ | ● | ◑ | ◑ | ◑ | ● | ◑ | ◑ |
| Normal mode | ● | ◑ | ● | ◑ | ● | ◑ | ◑ | |
| Wavenumber integration | ● | ◑ | ● | ◑ | ◑ | ◑ | ◑ | ◑ |
| Energy flux | ● | ◑ | ● | ◑ | ◑ | | ◑ | |
| Hybrid normal mode energy flux | ● | ◑ | ● | ◑ | ● | ◑ | ● | ◑ |

| | |
|---|---|
| | Not suitable |
| ◑ | Limited in accuracy or speed of execution |
| ● | Accurate and practical |

## 2.2.2. Parabolic equation models

From Table 2, as stated, parabolic equation models are a good fit for modelling the radiated sound field from marine impact piling. The parabolic equation method presumes that the energy travelling away from the source is substantially greater

than any back-scattered energy, such that one solves an outgoing wave equation rather than a more complicated elliptic boundary-value problem. Consequently, the computation is easier and typically has negligible accuracy loss due to the slowly varying environments commonly encountered in oceanic situations. Range dependency is implemented by simply representing the region as a series of range-independent regions, with a level of accuracy dictated by the resolution of these subregions.

One such implementation of the parabolic equation method is the Range-dependent Acoustic Model (Collins 1993), commonly referred to as RAM. One aspect is the initial condition, or the sound field very close to the source location, which includes a singularity at the source depth representing the point source. Unless other allowances are made, RAM calculates the sound propagation from a single point source and requires a specified depth for this point from which sound is emitted.

In the reviewed EIAs, the authors state that the model used is based on RAM but provide no source depth for the point source, or any suggestion that modifications had taken place to implement a line source. The reference for the model (Farcas et al. 2016), however, makes the assertion that "…this point source approximation can still produce reasonable predictions even for large sources such as monopiles or ships", and refers to a source depth in the text indicating that the model used was a point source model.

### 2.2.3. Energy flux models

Another approach to calculating the losses associated with the propagation of sound is presented in the work by Weston (1976). By making a number of simplifications, including uniform sound speed profile, a lossless medium, smooth and slowly-varying bathymetry, and source and receivers far from the boundaries, a set of equations are defined that specify propagation loss in four regions: spherical spreading, channelling or cylindrical spreading, mode-stripping, and single-mode. As the equations do not increase the number of calculation steps with increasing frequency it is often substantially faster at higher frequencies than more complex models.

The equations describing Weston's original model are based on the energy flux method and provide depth-independent (i.e., depth-averaged) results only. Given the requirement of a uniform sound speed, these solutions are often limited to shallow waters where water column refraction effects are negligible. Bathymetric variations are included in the form of an effective water depth, which is one that would generate the same combined reflection losses at a given range as the true bathymetry.

The approach by Weston has been extended to include consideration of the source and receiver depths and the effects of ray convergence from sea water refraction (Harrison 2013, Sertlek and Ainslie 2014). Hybrid modelling approaches such as combinations of normal mode and energy flux models can provide a similar accuracy to incoherent mode sum for the range dependent environments without requiring

long computational times (Sertlek et al. 2019). While the original work of Weston presumes an omnidirectional source, the energy flux method has been extended to a source with directivity in the sagittal plane (de Jong et al. 2019). This was originally introduced in the work by Zampolli et al. (2013) which included directivity in the form of the Dirac delta function limiting propagation to a single angle, i.e., that of the conical Mach wave. This formulation of the energy flux equations, limiting sound propagation to a single angle, was further elaborated into the DCS model (Lippert et al. 2018).

Consequently, similarly to RAM, energy flux models can be used to accurately predict the sound propagation provided the assumptions in its used are valid. The original derivations in Weston (1976), and referenced to in the Berwick Bank EIA (Seiche Ltd, 2022), are based on an omnidirectional source, i.e., a point-source model. While there exist modelling developments that take the unique nature of the impacted pile source into account, they do not appear in the EIAs reviewed as part of this project.

## 2.3. Review Summary

This section has provided an overview of the ECF as applied to piling, and the point-source equivalent ECF used in the reviewed reports, as well as some of the background to the source prediction and propagation methods. There are concerns with two separate aspects of the adopted approaches in models using the point-source equivalent ECF.

Firstly, with regards to the sound propagation, although validated and well-established models are used, the lack of consideration for the source geometry will lead to inaccuracies in the outputs; the illustrative differences between propagation from a point and from a line is discussed extensively in Section 3.

Secondly, presuming Equation 1 to be an appropriate method, the selection of point-source equivalent ECF is somewhat arbitrary. A limited number of calculations of the ECF have yielded results from 0.17 % (Dahl and Dall'Osto 2017) to 1.56 % (Dahl and Reinhall 2013), which equates to a range of 9.6 dB. The difference between values of $\beta$ of 0.5 % and 1.56 % is 4.9 dB, indicating that equivalent source levels may be underpredicted by that much based on the small set of calculated ECF values.

Using undocumented methods, point-source equivalent ECF values have been calculated to be as high as 13 % (Thompson et al. 2020). There has been little attempt to determine the factors controlling the point-source equivalent ECF, and any relative importance of the possible inputs. Additionally, even whilst restricting values of the point-source equivalent ECF to 0.5 % and 1.0 %, there are examples of very large differences in the distances to modelled isopleths corresponding to sound level thresholds.

# 3. Sound Propagation from Point and Line Sources

As noted in the derivation of the source energy formula, there is a difference between the nature of sound propagation from a point and from a line. This section investigates the differences between the two firstly using geometrical models to provide a general overview of the differences, and secondly using numerical modelling of a basic benchmark scenario.

## 3.1. Geometrical Sound Propagation Models

The propagation of sound depends on many factors that typically require detailed modelling to assess accurately. However, in many cases geometrical models provide very useful insight into the nature of sound propagation, and providing they are used appropriately, can provide accurate results of losses with increasing distance from the source.

In deep water, for example, basing sound propagation loss, $N_{\mathrm{PL}}$, on spherical spreading, i.e.,

$$N_{\mathrm{PL}}(r) = 20 \log_{10} \frac{r}{r_0} \text{ dB} \tag{17}$$

is a reasonable approximation up to distance where reflections from the seafloor become important.

In shallow water, which is more typical for piling, there exist simple expressions for propagation and transmission losses that take the shallow wave guide into consideration.

It is useful to distinguish between propagation loss and transmission loss. Both terms are defined in ISO 18405:

**propagation loss**:

the "*difference between source level in a specified direction and mean-square sound pressure level at a specified position*", and;

**transmission loss**:

the "*reduction in a specified level between two specified points $\boldsymbol{x}_1$, $\boldsymbol{x}_2$ that are within an underwater acoustic field*".

As described, the impacted pile does not have a source level, and consequently it is meaningless to use propagation loss in the calculation of received levels. Therefore, one needs to use transmission loss to characterise the change in level of the sound field with distance in the presence of the impacted pile.

### 3.1.1. Geometrical shallow water point source models

This section draws from work by Ainslie et al. (2014) from the conference paper "Practical Spreading Laws: The Snakes and Ladders of Shallow Water Acoustics" and presents the formulae for shallow water propagation loss when considering both monopole and dipole sources.

If one considers a point source, positioned in the water column suitably far from any boundaries, the initial sound propagation is in spherical shells located at the source. Consequently, sound propagation close to the point source is characterised by spherical spreading. In equation terms, the propagation loss, $N_{\mathrm{PL}}$, is

$$N_{\mathrm{PL}} = 10\log_{10}\frac{s^2}{r_0^2}\ \mathrm{dB} = 20\log_{10}\frac{s}{r_0}\ \mathrm{dB}, \tag{18}$$

where $s$ is the distance between the acoustic centre of the source and the receiver.

At greater distances from the source, the sea floor and sea surface have increasing influence over the sound field. The area through which the sound propagates becomes $2\pi rH$ where $r$ is the horizontal distance from the source and $H$ is the water depth. However, only sound propagating at angles less than the critical angle, $\psi$, contributes to this cylindrical spreading region. This yields a vertical aperture angle of $2\psi$ and a propagation loss of

$$N_{\mathrm{PL}} = 10\log_{10}\frac{r}{r_0}\mathrm{dB} + 10\log_{10}\frac{H/(2\psi)}{r_0}\ \mathrm{dB}. \tag{19}$$

Here, the $10\log_{10}(r)$ term dictates this to be cylindrical spreading.

With additional bottom reflections, energy propagating at steeper angles become more rapidly dissipated than those travelling close to horizontal. Consequently, the effective aperture angle decreases with range and can be expressed as

$$\theta_{\mathrm{eff}} = \left(\frac{\pi H}{4\eta r}\right)^{\frac{1}{2}}, \tag{20}$$

where $\eta$ is the gradient of seabed reflection loss with angle in units of nepers per radian (Np/rad).

Replacing $2\psi$ with the effective range-dependent aperture angle provides a propagation loss of

$$N_{\mathrm{PL}} = 10\log_{10}\frac{r^{3/2}}{r_0^{3/2}}\mathrm{dB} + 10\log_{10}\frac{\left(\frac{\eta H}{\pi}\right)^{1/2}}{r_0^{1/2}}\mathrm{dB}\,. \tag{21}$$

Here, the $10\log_{10}(r^{3/2}) = 15\log_{10}(r)$ corresponds to the standard mode-stripping formula.

These three propagation loss equations illustrate the three different regions of spreading involved in sound propagation from a point source comprising spherical spreading, cylindrical spreading, and mode-stripping (or intermediate) spreading.

Whilst there are simplifications and assumptions involved, they are accurate enough for many applications, particularly in favourable environments or for continuous sources operating over a narrow band of frequencies suitably far from the boundaries.

For point sources close to the boundary, Ainslie et al provide similar equations representing the point as a dipole source. Here, the point source sound field is strongly influenced by the reflected sound field, with the reflection providing a phase shift of 180° which gives rise to a Lloyd mirror interference pattern.

Figure 7 shows the propagation loss for a monopole point source calculated using the equations above.

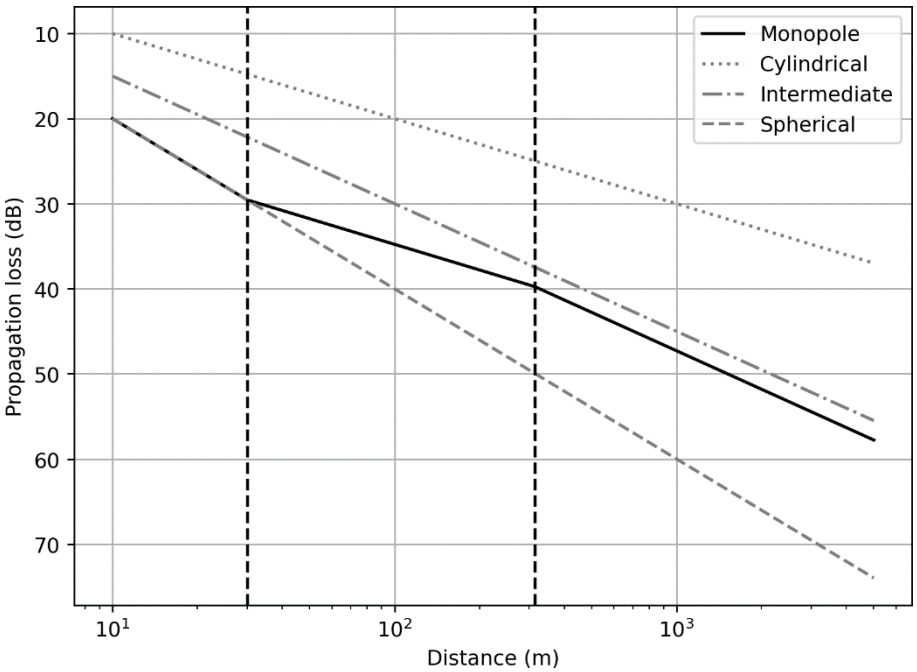


Figure 7. Example propagation loss (dB re 1 m²) from the geometric spreading equations for a point source in shallow water. Here, $H$ = 30 m, $\psi$ = 0.5 rad, and $\eta$ = 0.3 Np/rad. The vertical lines indicate the transitions from spherical to cylindrical, and cylindrical to mode-stripping regimes.

### 3.1.2. Damped cylindrical spreading

The impacted pile, as an acoustic source, behaves rather differently from a point source. The sound generation starts with the hammer impact at the top of the pile. This creates a compressive wave that travels down the pile at the compressive wave speed of steel. Associated with this wave is a localised radial expansion at the pile wall resulting in an acoustic wave travelling from the pile wall outwards. Taking the entire wetted pile length as the radiating surface results in conical wavefronts, or 'Mach' waves, the angle of which is dictated by the relative speeds of the compressional wave in water and steel.

The wavefronts radiate from the pile travelling at the angle of the cone. The sound then bounces between the seafloor and the sea surface losing energy with each reflection. As the energy of interest exists across the entire water column and is contained within it, the propagation resembles that of cylindrical spreading. The repeated bounces, however, provide an attenuation in level that is proportional to the distance from the pile.

The DCS model (Lippert et al. 2018) characterises the sound propagation based on the physical description. One important aspect to note, however, is that because source levels do not exist for piling, use of the term propagation loss in this context is meaningless. It therefore makes more sense to use transmission loss, described above as the change in sound level between two points in an acoustic field.

The transmission loss between points at ranges $r$ and $r_1$ from a source is given by

$$\Delta L_{\mathrm{TL}}(r; r_1) = L_E(r_1) - L_E(r)\,, \tag{22}$$

where $L_E$ is the sound exposure level. For sound radiated by the pile, the sound energy is spread into an area of $2\pi r H$, where $H$ is the water depth; this corresponds to cylindrical spreading. In addition to this, there is the energy loss from multiple boundary reflections causing exponential decay. With these two elements, the DCS model can be written as

$$\Delta L_{\mathrm{TL}}(r; r_1) = 10 \log_{10} \frac{r}{r_1} \mathrm{dB} + \alpha\,(r - r_1)\,, \tag{23}$$

where the horizontal decay rate, $\alpha$, is given by

$$\alpha = -\frac{10 \log_{10} |R|^2 \ \mathrm{dB}}{r_c}\,, \tag{24}$$

$R$ is the plane wave reflection coefficient, and $r_c$ is the horizontal distance between successive bottom reflections.

The DCS model has been validated against measurements that has found good agreement up to a limiting range dictated by the attenuation coefficient (Ainslie et al. 2020). The maximum usable range of Equation 23 is dictated by the $\alpha$ term. Where $\alpha r$ becomes large the amplitude of the Mach cone becomes negligible compared to the near-horizontal paths that are initially much weaker. An upper limit of $\alpha r < 20$ dB has been suggested based on measurements, after which an extrapolation scheme using $25 \log_{10}(r)$ is applied (Heaney et al. 2020).

An example of transmission loss calculated using the DCS model is shown in Figure 8.

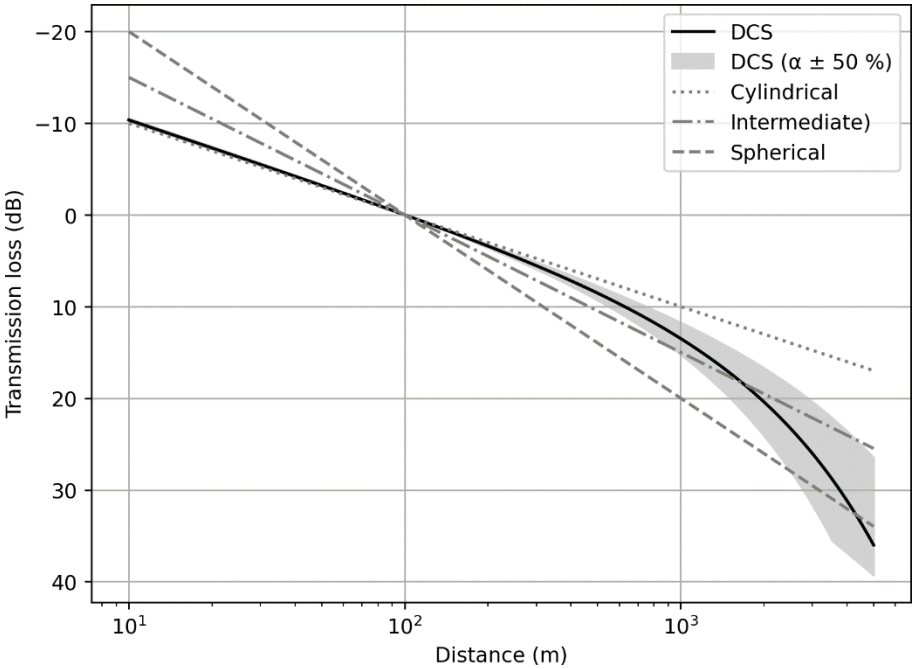


Figure 8. Example transmission loss referencing the sound level at 100 m using the DCS model. Here, the water depth, $H$, is 30 m, and the reflection loss coefficient, $R$, is 0.92. Results are shown for ±50 % of the calculated horizontal decay rate. The upper limit of 20 dB has been applied to the $\alpha r$ term, leading to the change in the slope for the lower bound of DCS beyond 3 km.

### 3.1.3. Comparison of point monopole source propagation and DCS

Given the differences in the nature of propagation between the point source and the DCS model it is informative to provide a direct comparison. Here, we consider three basic examples illustrating how the curves can diverge.

In the first example, we consider a situation featuring a sound source in a water depth of 30 m. Figure 9 shows the transmission loss curves calculated using the monopole model, and the DCS model presuming a reference distance of 100 m from the source in a best-case scenario. In this instance, the propagation from the monopole source is in the cylindrical spreading region, and consequently the curves match reasonably well from 30 to 1000 m. The differences near the source are due to the spherical spreading regime of the monopole, and differences at greater distances are caused by the increasing significance of the absorption term in the DCS model. Level differences at 1, 100, and 5000 m are shown in Table 3.

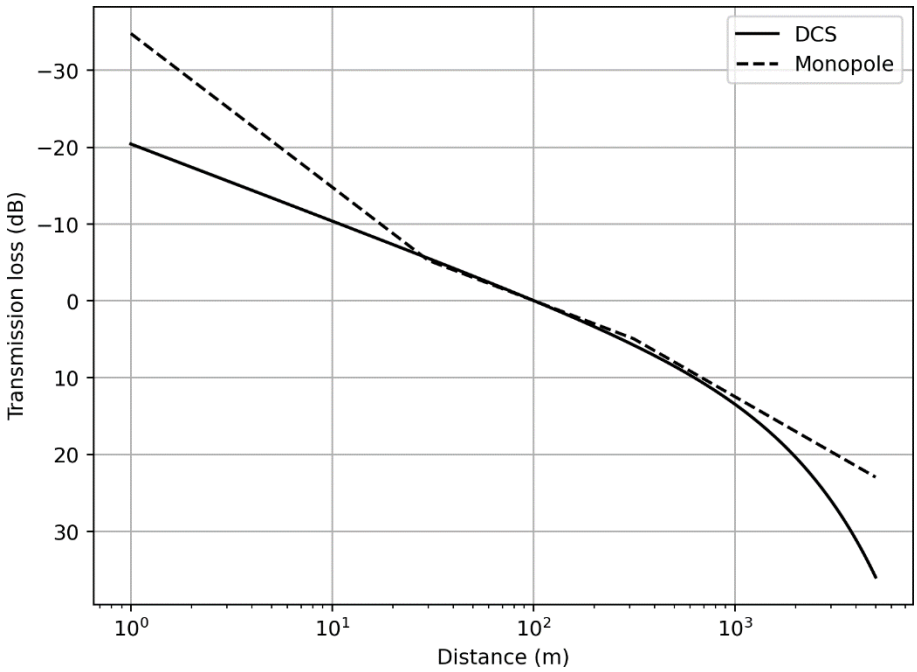


Figure 9. Transmission loss referencing the sound level at 100 m calculated for a monopole point source and DCS model in 30 m water depth. Although levels around the reference point match well, back-propagating or forward-propagating sound levels results in increasingly large errors.

Table 3. Calculated transmission loss (dB) between the monopole and DCS models for Example 1.

| Distance from source (m) | Monopole $\Delta L_{\mathrm{TL}}$ | DCS $\Delta L_{\mathrm{TL}}$ | Difference in $\Delta L_{\mathrm{TL}}$ |
|---|---|---|---|
| 1 | -34.8 | -20.4 | 14.4 |
| 100 (reference) | 0 | 0 | 0 |
| 5000 | 23.0 | 36.0 | 13.0 |

The second example considers the effect of increasing the water depth to 100 m, with all other parameters kept constant. The reference point again is 100 m. Figure 10 shows the transmission loss relative to the sound level at 100 m for this deeper case. Here, the deeper water results in the point source propagation to exist in the spherical spreading regime for longer, such that sound levels close to the source diverge more between the two models than for the previous example. The cylindrical spreading region for the point source model starts at 100 m. Due to the deeper water, the propagating wave from the pile experiences fewer reflections for a given distance such that the absorption term is reduced; this results in the two curves agreeing over a longer distance. Inevitably, however, at increasing distances the absorption term in the DCS model dominates such that at greater ranges the point source model still overpredicts the sound levels. Calculated transmission losses for select points are shown in Table 4.

Table 4. Calculated transmission loss (dB) between the monopole and DCS models for Example 2.

| Distance from source (m) | Monopole $\Delta L_{\mathrm{TL}}$ | DCS $\Delta L_{\mathrm{TL}}$ | Difference in $\Delta L_{\mathrm{TL}}$ |
|---|---|---|---|
| 1 | -40.0 | -20.1 | 19.9 |
| 100 (reference) | 0 | 0 | 0 |
| 5000 | 20.4 | 22.7 | 13.0 |

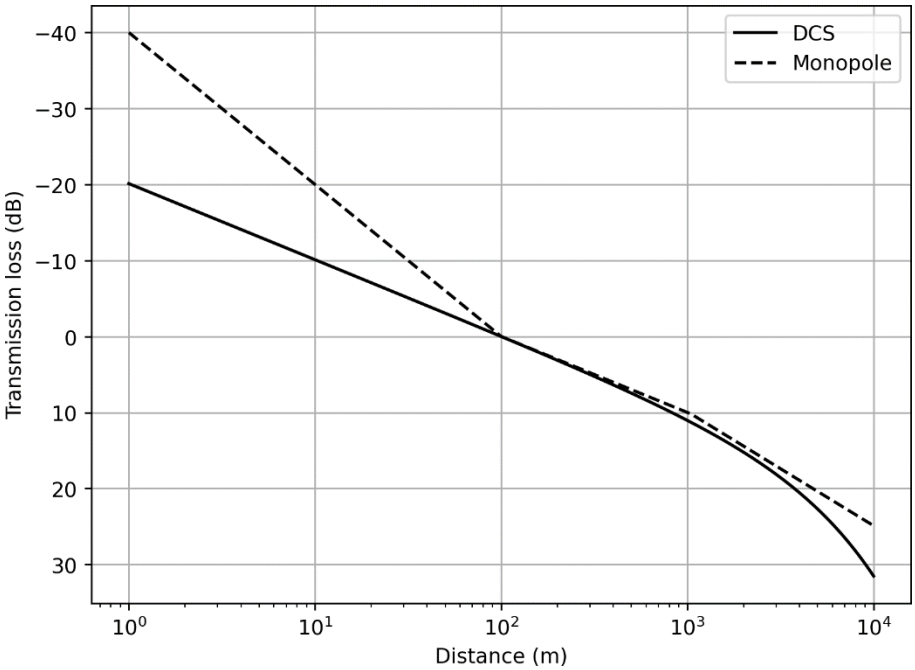


Figure 10. Transmission loss referencing the sound level at 100 m calculated for a monopole point source and DCS model in 100 m water depth. Although levels around the reference point match well, back-propagating or forward-propagating sound levels results in increasingly large errors.

The third and last example to be considered here illustrates how different circumstances, taking different reference points and different environments, can lead to different outcomes. Using a reference distance of 2 km, and a water depth of 15 m, whilst keeping everything else constant results in the curve seen in Figure 11. Here, there are substantial differences between the nature of sound propagation between the two models leading to significant errors if one were to use the incorrect method as shown in Table 5.

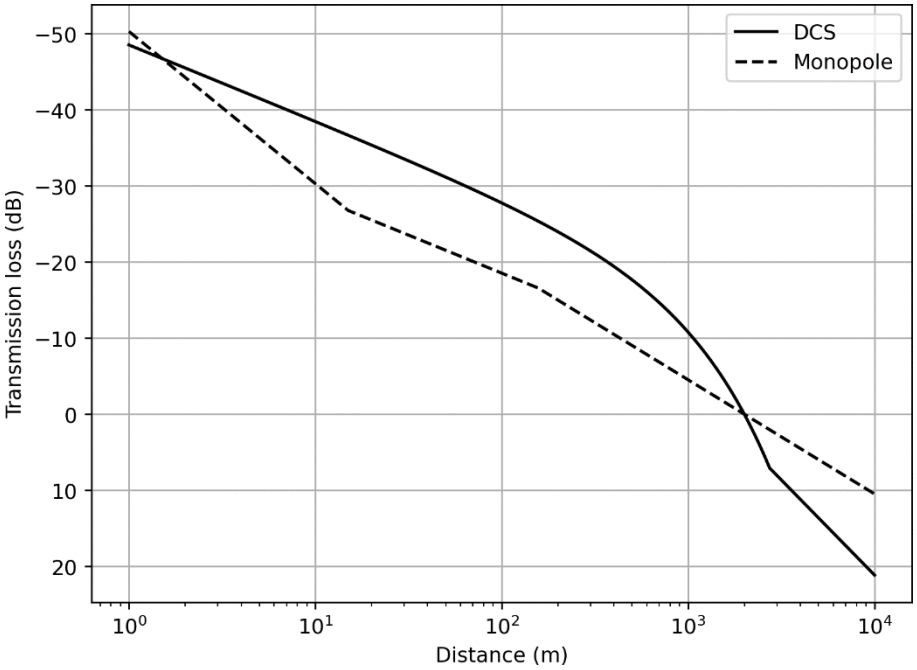


Figure 11. Transmission loss referencing the sound level at 2 km calculated for a monopole point source and DCS model. Whilst the curves match near the source and at the reference point, there are large differences in between.

Table 5. Calculated transmission loss (dB) between the monopole and DCS models for Example 3.

| Distance from source (m) | Monopole $\Delta L_{\mathrm{TL}}$ | DCS $\Delta L_{\mathrm{TL}}$ | Difference in $\Delta L_{\mathrm{TL}}$ |
|---|---|---|---|
| 1 | -50.3 | -48.5 | 1.8 |
| 100 | -18.5 | -27.7 | -9.2 |
| 5000 | 6.0 | 13.7 | 7.7 |

We present a worked example of sound level predictions when using two of these transmission loss curves. In the first example, with 30 m water depth and a reference distance of 100 m, if the measured SEL was 190 dB, the predicted theoretical levels at 1 m would be 224.8 dB for the monopole source compared to 210.4 dB from the DCS model. Similarly, at 5 km, the monopole model would generate an SEL of 167.0 dB compared to 154.0 dB from the DCS models.

Often the primary output from the modelling comprises predictions of distances at which sound levels drop below specified threshold levels as shown in Table 6. It is noted that the results presented here all consider just the broadband sound level, i.e., no frequency-weighting has been applied. Using the first example from Figure 9, comparing distances to where the SEL drops to 180 dB, the monopole provides 690 m compared to 640 m from the DCS model. However, a similar comparison where the SEL drops below 170 dB yields 3.1 km for the monopole compared to

2.0 km from the DCS model. The differences in this case, increase as one moves further from the reference distance.

In the shallow water case in the third example shown in Figure 11, if one were to presume a measured SEL of 170 dB at 2 km, the result at 1 m is 220.3 dB for the monopole and 218.5 dB for the DCS model. Whilst the similarity in levels at this distance looks encouraging, the intervening SEL results depart substantially from one another. At 100 m, we see a predicted SEL from the monopole model of 188.5 dB but 197.7 for the DCS model. Again, looking at distances to where the SEL drops below a certain value (Table 7), for 190 dB the distances are 73 m for the monopole model and 370 m for the DCS model; for 180 dB, these are 430 m and 1.1 km respectively.

Table 6. Calculated distances to arbitrary SEL thresholds (dB re 1 μPa²s) for the monopole and DCS models for Example 1.

| SEL threshold (dB) | Monopole model distance (m) | DCS model distance (m) |
|---|---|---|
| 190 (reference) | 100 | 100 |
| 180 | 693 | 640 |
| 170 | 3183 | 1950 |

Table 7. Calculated distances to arbitrary SEL thresholds (dB re 1 μPa²s) for the monopole and DCS models for Example 3.

| SEL threshold (dB) | Monopole model distance (m) | DCS model distance (m) |
|---|---|---|
| 190 | 73 | 374 |
| 180 | 434 | 1084 |
| 170 (reference) | 2000 | 2000 |

The examples above illustrate the need to use an appropriate model for each situation. We have not presented any results using the dipole source geometric model; however, given the varied spreading regimes, it is clear that the end result would show that this is also very different from the DCS model. It is noted that while the geometric model differs from the DCS model, more sophisticated point source modelling will generate more accurate answers for situations involving more complex environments and signals. To further illustrate that, despite this, the point source model is inadequate for piling predictions, we provide examples using numerical modelling in the next section.

## 3.2. Numerical Sound Propagation Modelling

While geometric models provide very quick answers and useful insight to the problem, it can be argued that they are not suited to all situations and that more sophisticated methods are required. This section provides two simple examples of numerical modelling results when considering propagation from both a point source and a line source.

### 3.2.1. Example scenario

The parameters used for the baseline scenario are selected to be broadly typical of a North Sea piling operation. The pile properties are shown in Table 8. The hammer selected for the study was an IHC S-2300 operating at its full capacity of 2300 kJ. The choice of hammer is based on using one that has been commonly used for monopile installation and is not intended to imply a recommendation.

Table 8. Parameters for the example pile.

| Parameter | Value |
|---|---|
| Pile length | 70.0 m |
| Pile diameter | 6.0 m |
| Pile wall thickness | 5 cm |
| Penetration depth | 20.0 m |

The environment comprised a 30 m column of water and flat bathymetry. The sound speed profile for the study is an isovelocity profile at 1490 m/s. The sediment is based on medium sand, with a grain size of 1.5 φ. The geoacoustic profile in Table 9 has been calculated using surficial sediment properties taken from Ainslie (2010) and depth-dependent equations from Hamilton (1980); shear wave properties are from general results by Holzer et al. (2005) and Buckingham (2005).

Table 9. Geoacoustic model for the numerical modelling example, which represents an increasingly consolidated sand bottom. Each parameter varies linearly with depth between entries.

| Depth below seafloor (m) | Material | Density (g/cm³) | Compressional wave | | Shear wave | |
|---|---|---|---|---|---|---|
| | | | Speed (m/s) | Attenuation (dB/λ) | Speed (m/s) | Attenuation (dB/λ) |
| 0 | Sand | 2.090 | 1784.7 | 0.88 | 300 | 3.65 |
| 100 | | 2.216 | 1908.0 | 0.85 | | |
| 200 | | 2.337 | 2017.9 | 0.81 | | |
| 300 | | 2.447 | 2116.2 | 0.76 | | |
| 400 | | 2.546 | 2204.2 | 0.71 | | |
| 500 | | 2.634 | 2283.6 | 0.66 | | |

#### 3.2.1.1. Line source modelling

To perform the numerical modelling for the phased line source JASCO's PDSM (MacGillivray 2014) was used. The process involves the following steps:

- Define the input forcing function at the head of the pile using GRLWEAP (Pile Dynamics 2010).
- Model the progression of the stress wave down the pile based on a finite-difference calculation of cylindrical shell equations, whilst taking the radiation damping of the water and sediment, and the pile toe reflection into account.
- Calculate the contributions of an array of monopoles located on the central axis that simulate the radiated sound field at the pile wall.
- An array starter method is used to generate a directional starting field at each frequency to fully take into account the geometry of the source.
- The starting field is propagated in distance using a parabolic equation model (described above).

Further details of the model used for the line source in this example are provided in Appendix A. The monopoles on the central axis were positioned 1 m apart, and the maximum frequency of the model was 1123 Hz (upper band edge of the 1 kHz decidecade band). The parabolic equation model used a frequency-dependent range step between 50 m at the lowest frequencies to 10 m at the highest; similarly, the depth step ranged from 0.5 m to 0.125 m.

Figures 12 and 13 show the per-pulse SEL field calculated by the line-source model over 1 km and 10 km respectively. In Figure 12, the path of the Mach wave, and associated shadow zone are visible at ranges up to approximately 150 m.

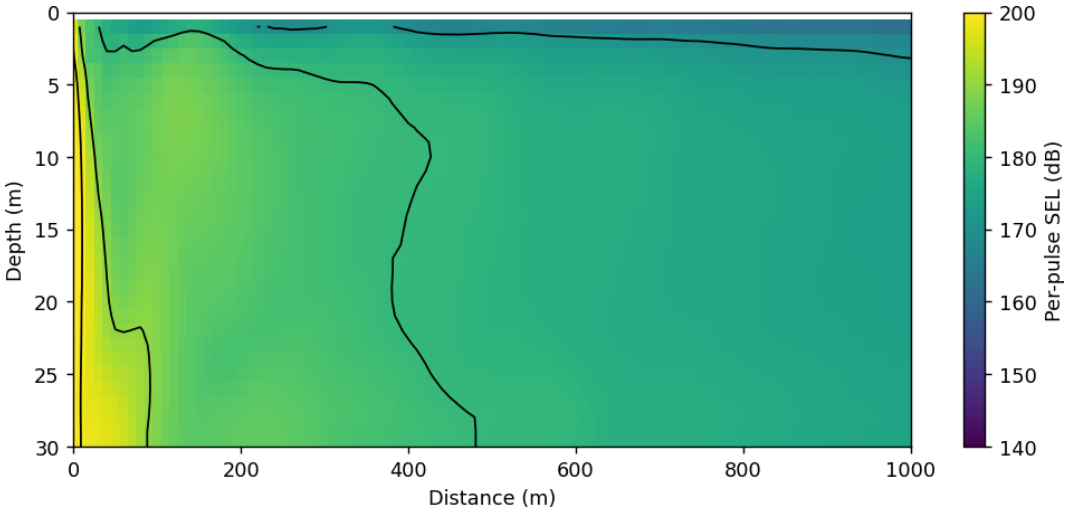


Figure 12. Per-pulse SEL (dB re 1 µPa²s) sound field up to 1 km generated by the line-source model for the example scenario.

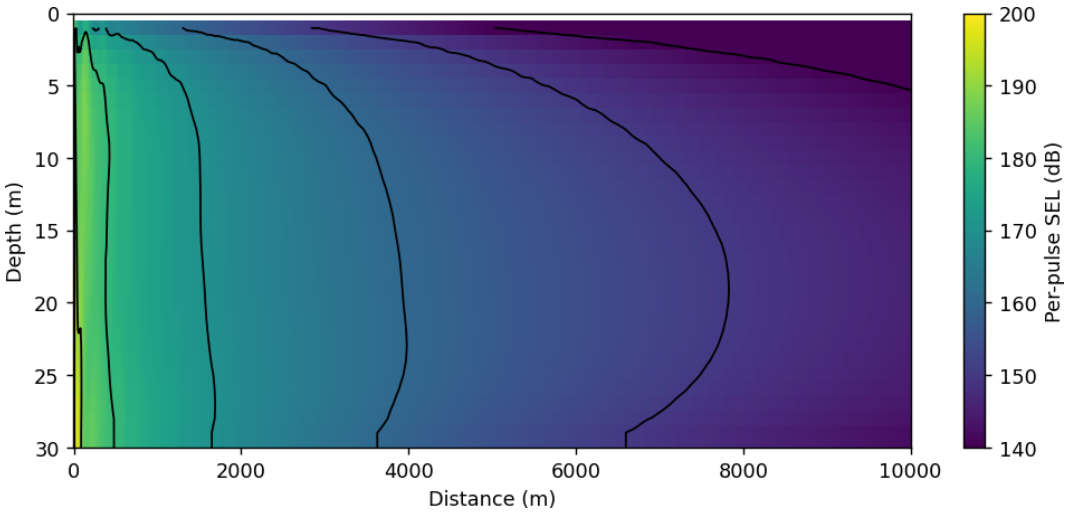


Figure 13. Per-pulse SEL (dB re 1 µPa²s) sound field up to 10 km generated by the line-source model for the example scenario.

Figure 14 shows the per-pulse SEL both for a receiver 2 m from the sea floor, the depth-averaged result, and the DCS model. As the DCS model only provides predictions of transmission loss, it is necessary to include a measured or modelled received level to generate full level against range results. In this case, sound levels were matched at 10 m from the pile, but it is evident that there would be small errors if the sound levels were matched at a point where the curves separate (i.e., 50 m or 150 m). Additionally, as stated in Section 3.1.2, the DCS model is less suited to greater ranges where the absorption term is great and other mechanisms giving rise to sound energy travelling near horizontally start to dominate; this is evident in the plot from approximately 4 km, with the empirical change to $25 \log_{10}(r)$ propagation starting from 5 km.

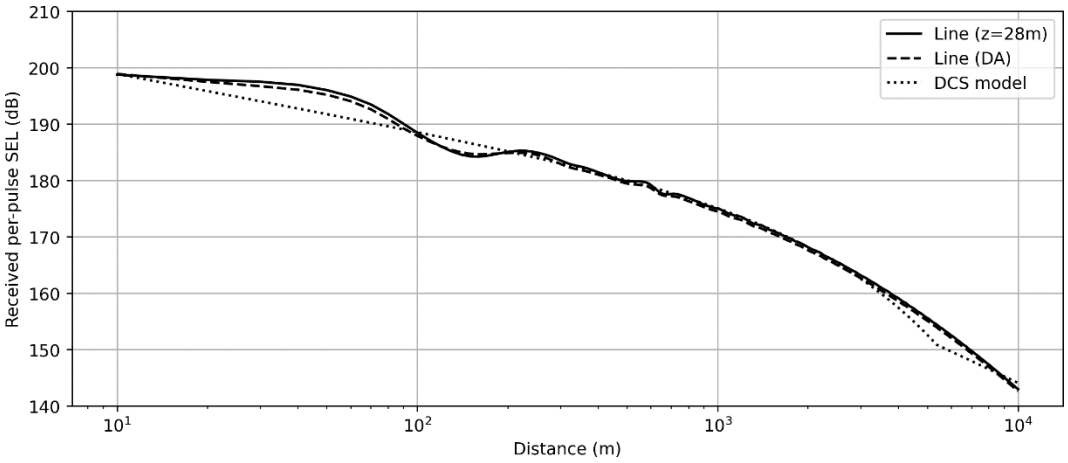


Figure 14. Per-pulse SEL (dB re 1 μPa²s) as a function of distance. Results are shown for a receiver 2 m from the seafloor (z = 28 m), the depth-averaged level, and the DCS model matching levels at 10 m.

#### 3.2.1.2. Point source modelling using sample measurements

Where measurements are available, a commonly used method for calculating the sound field is to take the result at the measurement point, back-propagate it to a source location, and forward-propagate in order to generate the full sound field. Results from Figure 14 suggest that when using an appropriate model, this approach may yield very reasonable outcomes. In this case, however, we investigate the effect of basing propagation loss on a point source assumption.

Point source propagation losses were calculated in RAM (see Section 2.2.2) for a source located at 15 m depth (i.e., mid-depth) for decidecade band centre frequencies from 10 Hz to 1 kHz for the environment described above. Results for the decidecade bands were generated from the single frequency propagation loss using a frequency averaging algorithm (Harrison and Harrison 1995).

Results are calculated for receivers located at 100 m and 170 m from the pile, both 2 m from the seafloor. Back-propagating for each decidecade band provides two very different source level spectra as shown in Figure 15. Whereas the structure of the sound field for the pile varies little with frequency (as energy is travelling in the fixed direction), the sound fields resulting from the point sources have more structure that varies with frequency. Consequently, in cases where incorrect propagation losses are used, it is possible to generate large differences between back-propagated source levels simply due to location of the measurement point. Here, we see source levels taken from 100 m receiver to be significantly higher than those for the 170 m receiver; additionally, the peak frequency has moved from the 160 Hz band to 63 Hz. The broadband source levels of the two results are shown in Table 10.

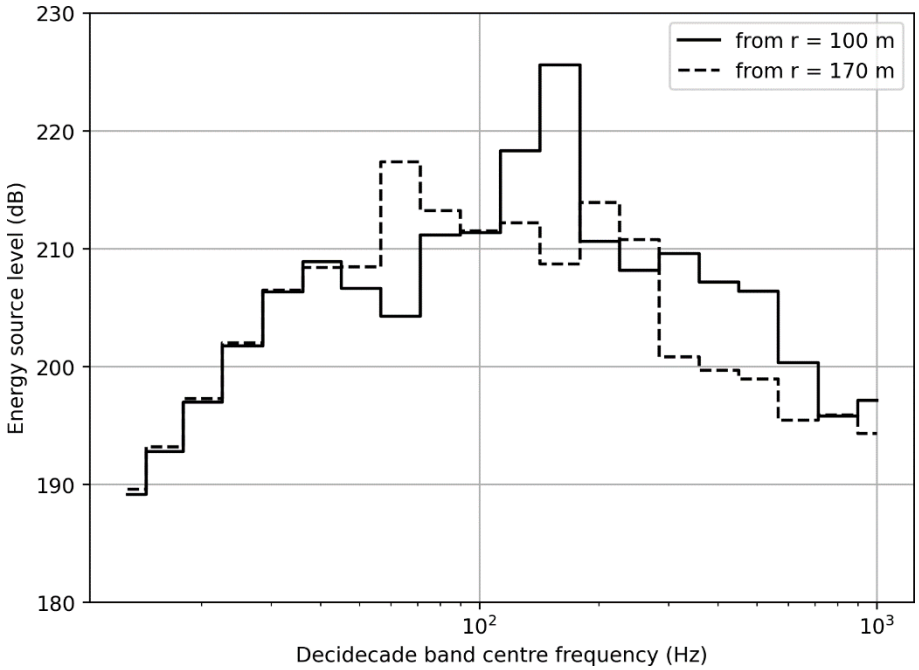


Figure 15. Back-propagated energy source levels (dB re 1 μPa²m²s) using the modelled sound field from the line source and propagation loss calculations for the point source.

Table 10. Broadband energy source levels (dB re 1 μPa²m²s) calculated using the back-propagating from a single point.

| Parameter | From 100 m | From 170 m |
|---|---|---|
| ESL (dB) | 227.2 | 222.4 |

Figures 16 and 17 show the calculated sound field up to 1 km and 10 km respectively for source levels calculated at 100 m. Similarly, Figures 18 and 19 show the calculated sound field up to 1 km and 10 km respectively for source levels calculated at 170 m.

Figure 20 shows the calculated per-pulse SEL taken at a depth of 28 m as a function of distance from the pile for the line-source and the two point-source outputs. Here, we note that the levels for the point source are matched to the line source at their respective distances. Figure 21 shows the equivalent depth-averaged results. Here we see a poor match for source levels calculated at 100 m, but a reasonable match for the first couple of kilometres for the source levels calculated at 170 m. For much of the range, the point source field is in the cylindrical spreading region, which is similar to the DCS model where the absorption term is still low. Once out of this region, however, the exponential losses apparent in the DCS model cause the curves to diverge. It's also worth noting that although in this case there was a reasonable match between the line source and the point source from 170 m levels, as shown, the back-propagated source levels can vary substantially based on the location from which they are calculated.

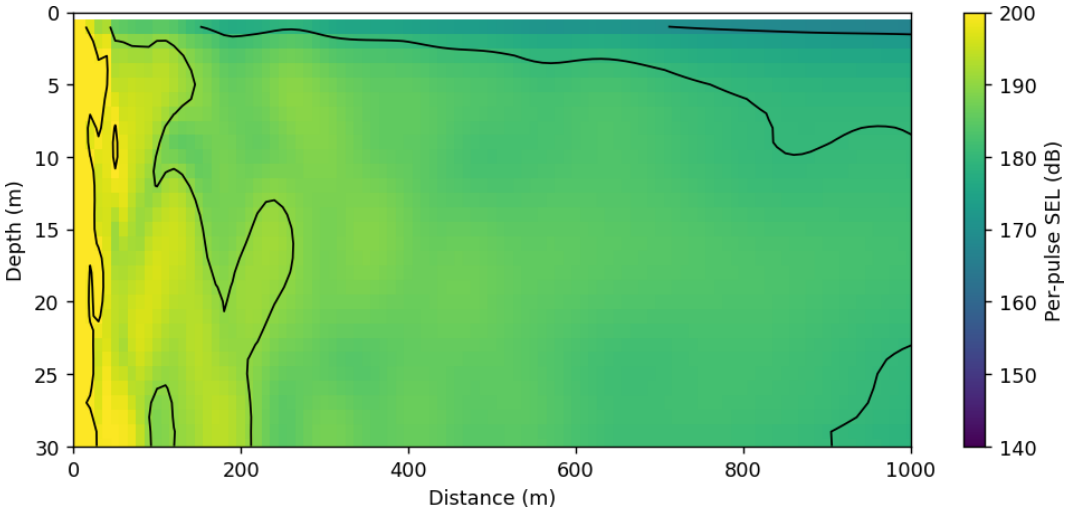


Figure 16. Per-pulse SEL (dB re 1 µPa²s) sound field up to 1 km generated by the point-source model for the example scenario, with levels back-propagated using levels from the line-source model for a receiver at 100 m range and 28 m depth.

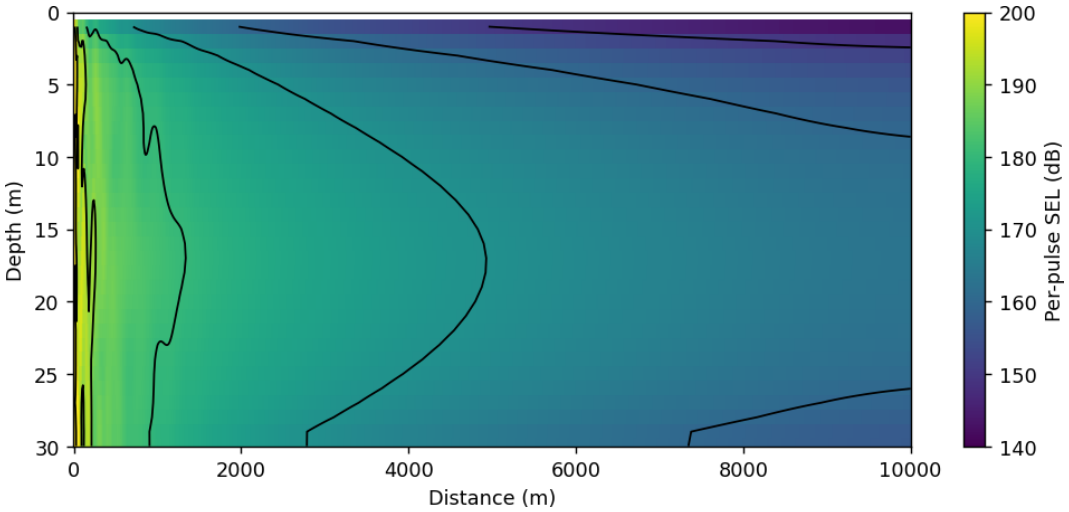


Figure 17. Per-pulse SEL (dB re 1 µPa²s) sound field up to 10 km generated by the point-source model for the example scenario, with levels back-propagated using levels from the line-source model for a receiver at 100 m range and 28 m depth.

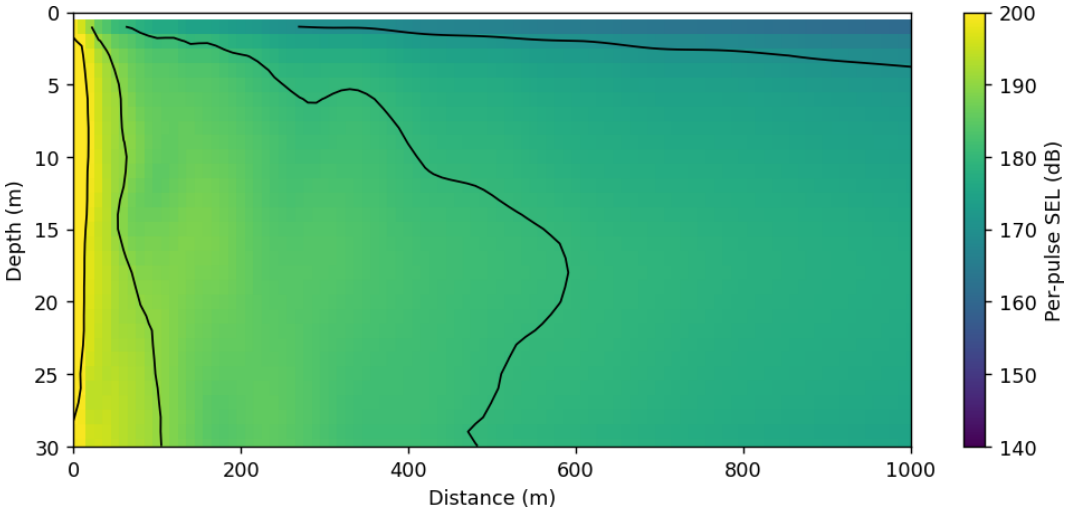


Figure 18. Per-pulse SEL (dB re 1 µPa²s) sound field up to 10 km generated by the point-source model for the example scenario, with levels back-propagated using levels from the line-source model for a receiver at 170 m range and 28 m depth.

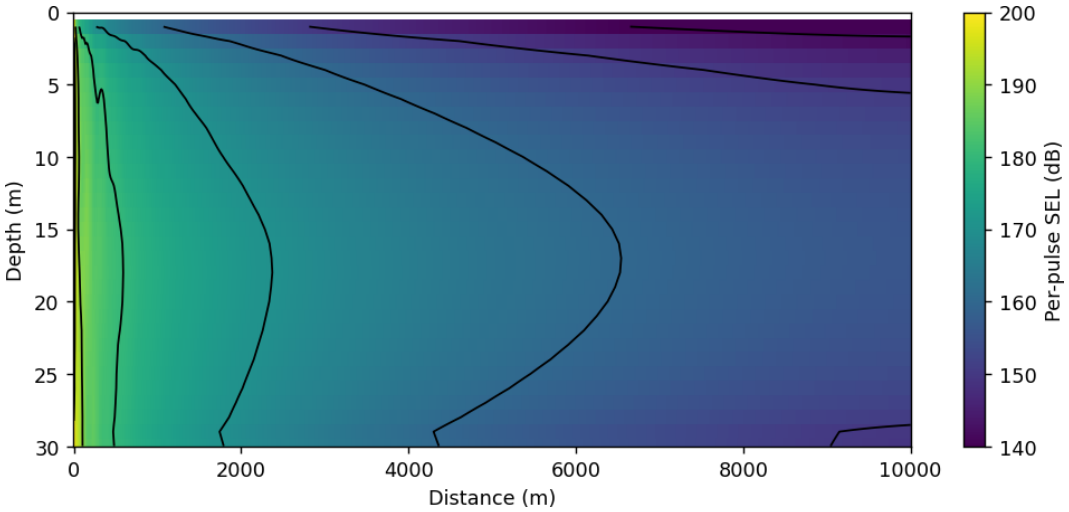


Figure 19. Per-pulse SEL (dB re 1 µPa²s) sound field up to 10 km generated by the point-source model for the example scenario, with levels back-propagated using levels from the line-source model for a receiver at 170 m range and 28 m depth.

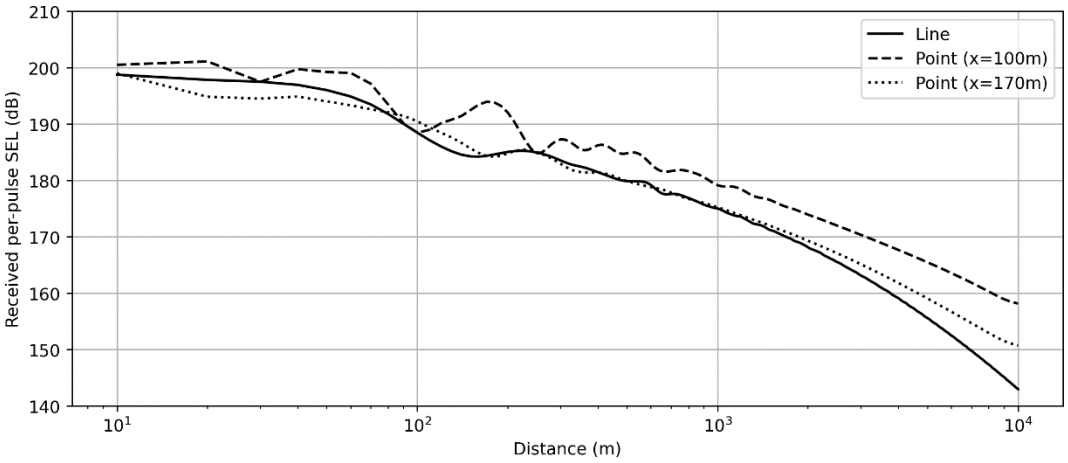


Figure 20. Per-pulse SEL (dB re 1 μPa²s) as a function of distance for line and back-propagated point sources. Results are shown for a receiver 2 m from the seafloor (z = 28 m).

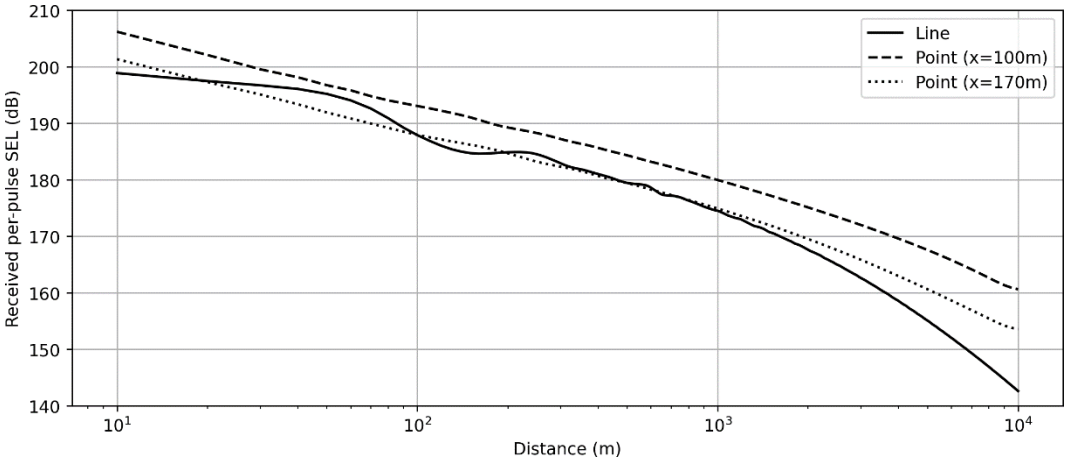


Figure 21. Depth-averaged per-pulse SEL (dB re 1 μPa²s) as a function of distance for line and back-propagated point sources.

### 3.2.1.3. Modelling using point-source equivalent ECF method

The final example presented in this section is for modelling using the point-source equivalent ECF method. Here the broadband energy source level is calculated using Equation 1, for the given hammer impact energy of 2300 kJ. The calculated energy source levels are shown in Table 11 for point-source equivalent ECFs of 0.5 % and 1.0 %.

Table 11. Broadband energy source levels (dB re 1 μPa²m²s) calculated using the point-source equivalent ECF method.

| Parameter | ECF: 0.5 % | ECF: 1.0 % |
|---|---|---|
| ESL (dB) | 211.5 | 214.5 |

The spectral shape of the source is taken from a figure of the source spectrum presented in Moray East underwater noise modelling report (Cefas 2019). The relative contribution between the frequency bands is constant, with levels offset to provide the broadband levels from Table 11. The resulting ESL spectra are shown in Figure 22.

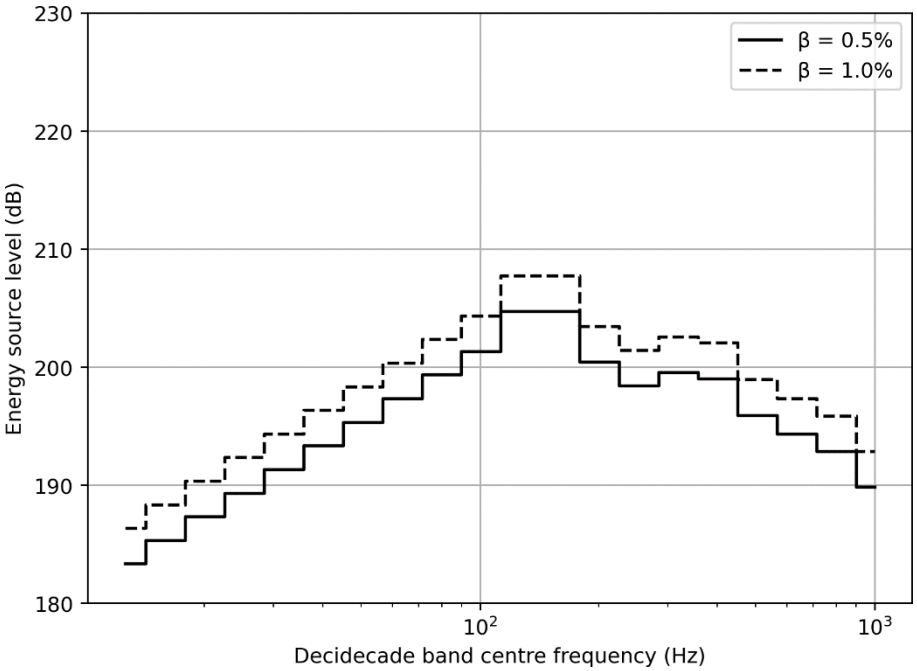


Figure 22. Energy source levels (dB re 1 µPa²m²s) calculated using the point-source equivalent ECF method for $\beta$ = 0.5 % and $\beta$ = 1.0 %.

Comparing the energy source levels between those generated using the point-source equivalent ECF method (Table 11) and those using the back propagated value (Table 10) shows that, in this particular case, the point-source equivalent ECF method generates substantially lower source levels.

The propagation loss calculations from the point source model in Section 3.2.1.2 were reused for the point-source equivalent ECF-derived source levels. Slice plots of the sound fields up to 1 km and 10 km from the pile for the $\beta$ = 0.5 % ECF source are shown in Figures 23 and 24, with equivalent results for $\beta$ = 1.0 % in Figures 25 and 26. Comparing against the equivalent results for the back-propagated sound levels, the point-source equivalent ECF method in this example produces substantially lower sound levels in the field.

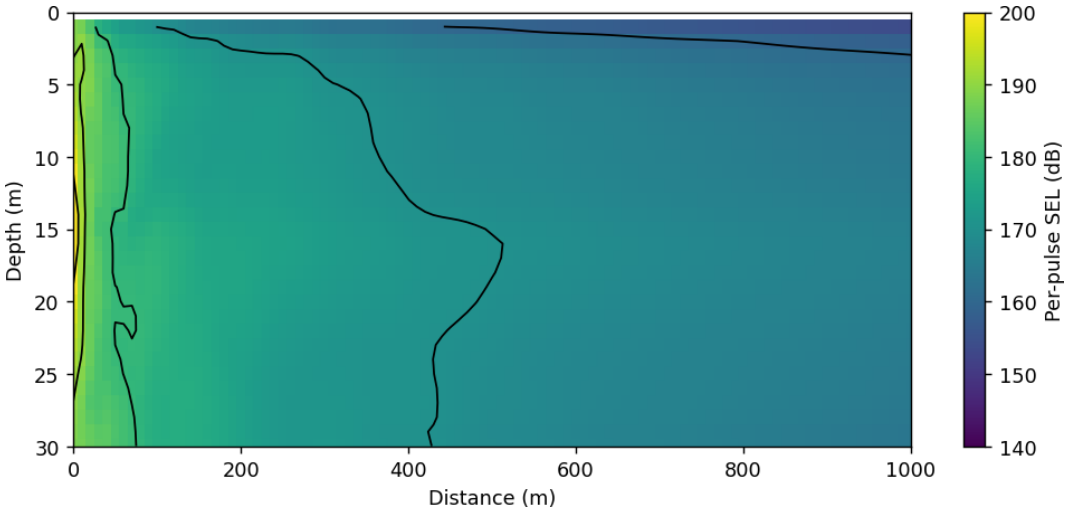


Figure 23. Per-pulse SEL (dB re 1 µPa²s) sound field up to 1 km generated by the point-source model for the example scenario, with levels calculated using a point-source equivalent ECF of 0.5 %.

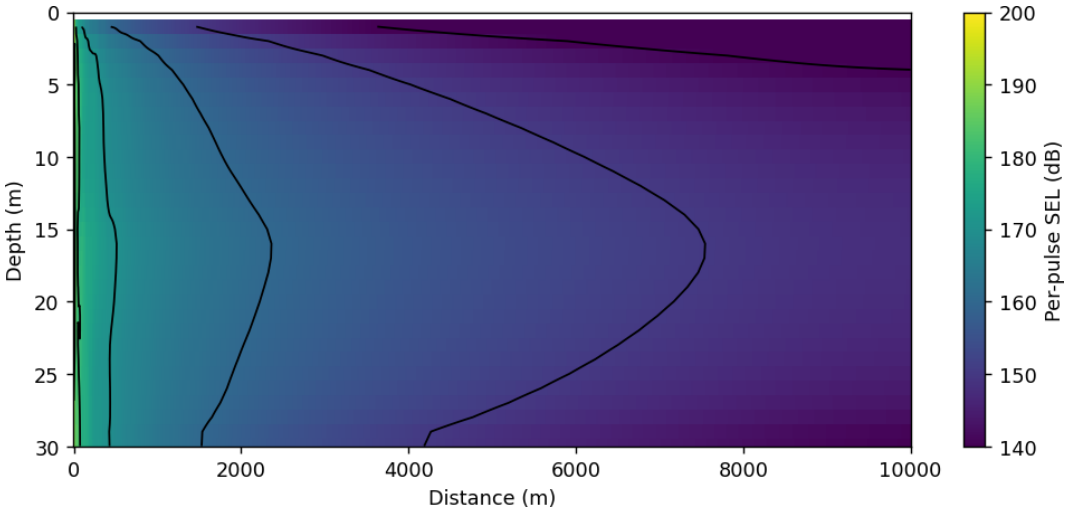


Figure 24. Per-pulse SEL (dB re 1 µPa²s) sound field up to 10 km generated by the point-source model for the example scenario, with levels calculated using a point-source equivalent ECF of 0.5 %.

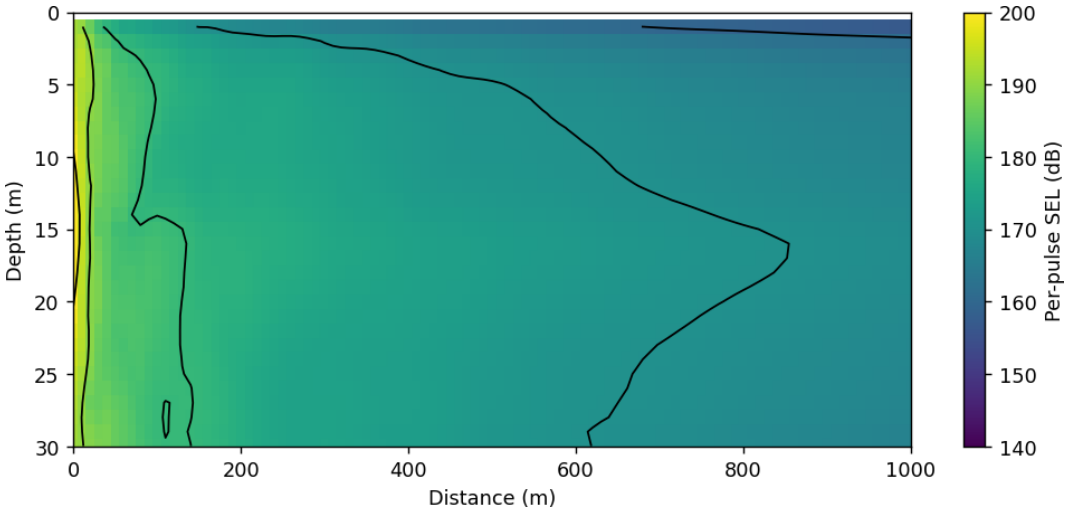


Figure 25. Per-pulse SEL (dB re 1 µPa²s) sound field up to 1 km generated by the point-source model for the example scenario, with levels calculated using a point-source equivalent ECF of 1.0 %.

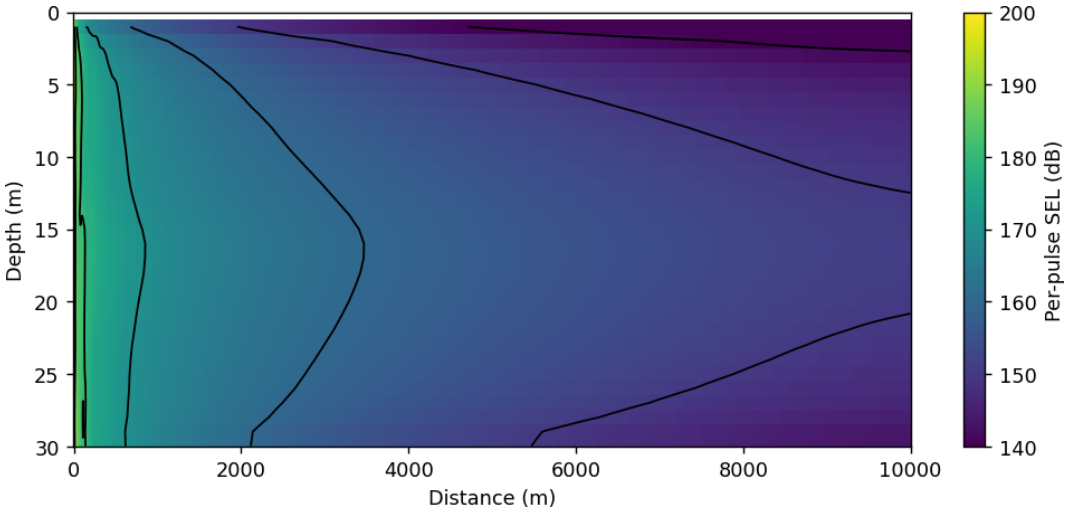


Figure 26. Per-pulse SEL (dB re 1 µPa²s) sound field up to 10 km generated by the point-source model for the example scenario, with levels calculated using a point-source equivalent ECF of 1.0 %.

Depth-averaged values for the two point-source equivalent ECF method results were calculated to compare against the line source model result and are shown in Figure 28. Here, we see large differences between the ECF results and the line source not only in terms of the sound level difference but also in the rate of decay as a function of range as shown in Figure 29.

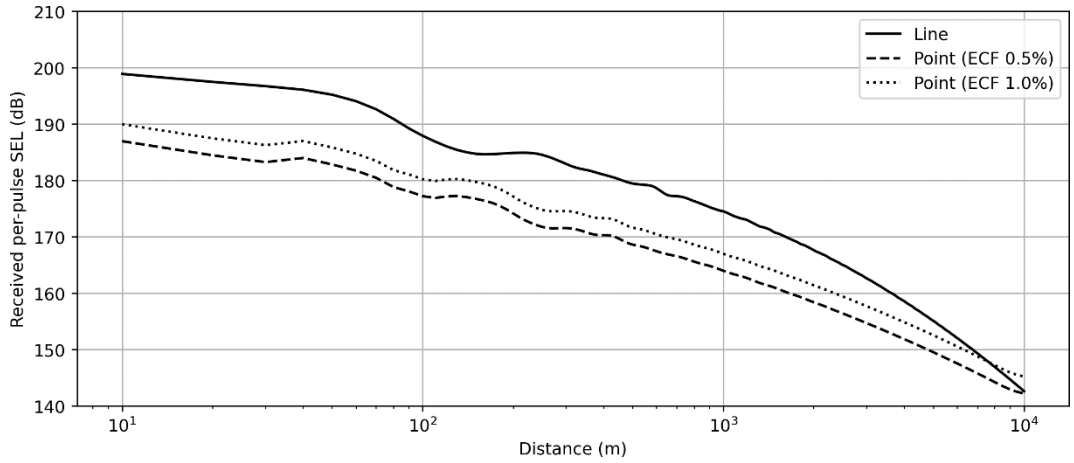


Figure 27. Per-pulse SEL (dB re 1 µPa²s) as a function of distance for line and point-source equivalent ECF model. Results are shown for a receiver 2 m from the seafloor (z = 28 m).

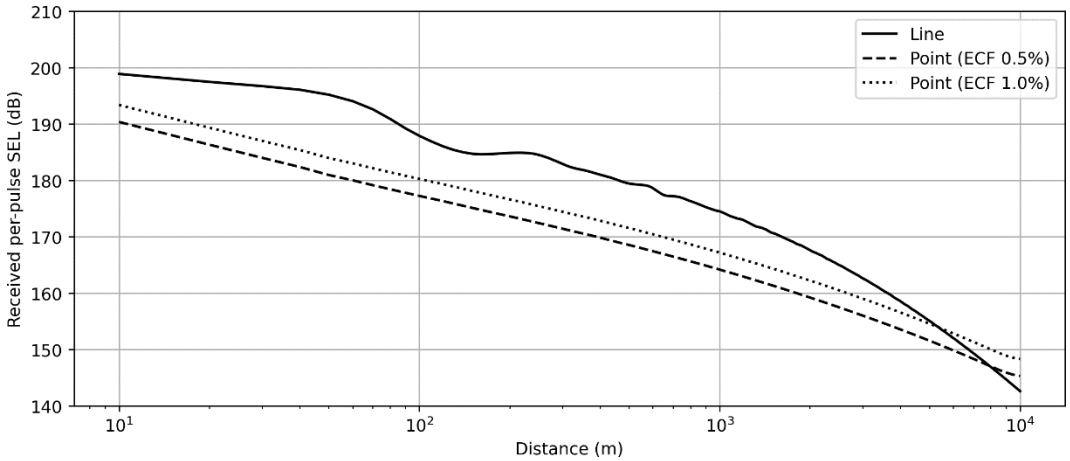


Figure 28. Depth-averaged per-pulse SEL (dB re 1 µPa²s) as a function of distance for line and point-source equivalent ECF model.

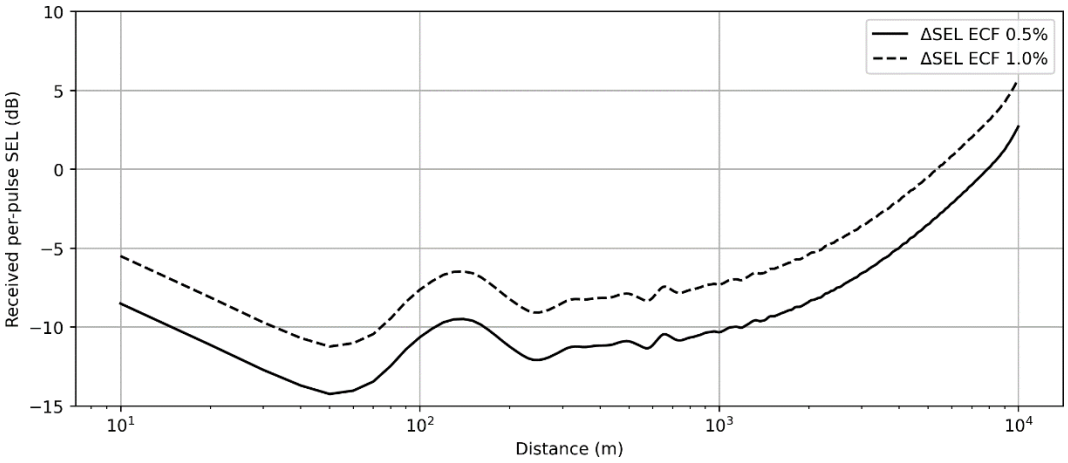


Figure 29. Difference in the per-pulse SEL against distance from the pile between the line source model and the point-source equivalent ECF model using $\beta$ = 0.5 % and 1.0 %.

### 3.2.1.4. Comparison of results

The methods presented in this section comprise a line-source model designed specifically to predict sound levels from piling, a point source model where there is a reference measurement at some point, and the same point source model using the point-source equivalent ECF method to generate source levels. In the case of using the DCS model, sound levels need to be obtained either from measurements or from a very similar previous study. The match against the line-source model, however, is good when taking a suitable reference point (Figure 14).

The point source examples using the refence sound level again illustrate the differences in the sound field between the different source assumptions. It also illustrates the possible differences that result from having a different reference location. In this case, the reference point of 170 m results in a reasonable match between the line and point source for the distances shown in the plot. This, however, should not lead one into thinking that this a suitable method, as taking a reference level at 100 m results in completely different propagation due to the implied prominence from different frequencies (see Figure 15). It is also evident that one cannot determine a good matching reference without having initially performed the appropriate modelling.

The point-source equivalent ECF method offers an alternate method of determining source levels directly without needing to back-propagate existing sound levels. Here, as previously described, spectral levels from measurements are increased or decreased in level to match a broadband ESL that is calculated from the hammer energy and the point-source equivalent ECF (Figure 22). In the example presented here, the broadband source levels for the point-source equivalent ECF method (211.5 and 214.5 dB) was substantially lower than either of those from the back-propagated results (227.2 and 224.0 dB). The result of this is that ECF model sound

levels in this example differ by 7 to 12 dB between 100 and 1000 m from the pile (Figure 29), and feature very different loss beyond 2 km.

As stated previously, a sought-after output of the modelling is often the distance at which sound levels drop below given thresholds. Table 12 provides an indication of the spread of values from the models in this example. It also highlights the importance of the source function used in the modelling; here we see the results from the ECF model falling far short of those from the other results when using the most commonly used values of the ECF.

Table 12. Distances (km) to specified sound exposure level thresholds (dB re 1 μPa²s) for the numerical models. Note that sound levels are not frequency weighted.

| Depth-averaged per-pulse SEL (dB) | PDSM | Point source | | | |
|---|---|---|---|---|---|
| | | Back-propagated ESL | | point-source equivalent ECF ESL | |
| | | $r = 100$ m | $r = 170$ m | β = 0.5 | β = 1.0 |
| 190 | 0.09 | 0.18 | 0.07 | 0.02 | 0.02 |
| 185 | 0.14 | 0.45 | 0.20 | 0.03 | 0.05 |
| 180 | 0.46 | 1.00 | 0.45 | 0.07 | 0.11 |
| 175 | 0.93 | 2.03 | 0.99 | 0.16 | 0.28 |
| 170 | 1.61 | 3.81 | 1.89 | 0.39 | 0.65 |
| 165 | 2.50 | 6.46 | 3.27 | 0.89 | 1.38 |
| 160 | 3.63 | >10.0 | 5.30 | 1.81 | 2.66 |

## 3.2.2. COMPILE II benchmark scenario

We briefly consider here a second modelled scenario based on the COMPILE II workshop scenario. The COMPILE II case was a real-life pile driving scenario with no noise mitigation measures, for which measurement data was made available after results submission for validating the acoustic models. Here, we present results generated by PDSM and those for the point-source equivalent ECF model with values for $\beta$ of 0.5 % and 1.0 % for the COMPILE II benchmark scenario.

### 3.2.2.1. Scenario description

The scenario describes a 75 m long pile, including a taper to bring the pile diameter from 5 m to 6.5 m over 20 m in the mid-section, being driven by a Menck MHU-3500S hammer. At the point of measurement, the blow energy was 1525 kJ and the pile had been driven 30 m. The water depth varies in accordance with Table 13 with participants instructed to obtain intermediate water depths through linear interpolation and assume constant bathymetry beyond the maximum distance. The pile was driven into layered sand and clay.

Table 13. Bathymetry in the COMPILE II scenario.

| Distance (m) | Water depth (m) |
|---|---|
| 0 | 39 |
| 245 | 39 |
| 747 | 37 |
| 1481 | 32 |

The sound speed profile for the study is an isovelocity profile at 1500 m/s. The geoacoustic profile (Table 14) was calculated from geological data provided for the workshop based on Buckingham's grain-shearing model (2005).

Table 14. Geoacoustic model calculated for the COMPILE II numerical modelling benchmarking scenario. Each parameter varies linearly within the stated depth ranges.

| Depth below seafloor (m) | Material | Density (g/cm³) | Compressional wave | | Shear wave | |
|---|---|---|---|---|---|---|
| | | | Speed (m/s) | Attenuation (dB/λ) | Speed (m/s) | Attenuation (dB/λ) |
| 0–5.0 | Loose to medium dense sand | 2.05-2.05 | 1696.0-1892.7 | 0.26-0.93 | 106.3-389.4 | 3.65 |
| 5.0–6.5 | Dense to very dense sand | 2.09-2.09 | 1912.9-1940.3 | 0.9-0.98 | 391.3-426.1 | |
| 6.5–9.0 | Sandy clay | 2.08-2.08 | 1707.3-1713.7 | 0.23-0.26 | 95.7-106.3 | |
| 9.0–11.5 | Dense to very dense sand | 2.09-2.09 | 1976.6-2008.9 | 1.08-1.16 | 475.4-515 | |
| 11.5–19.0 | Sandy clay | 2.08-2.08 | 1719.4-1732.3 | 0.28-0.33 | 115.9-136.2 | |
| 19.0–50.0 | Very dense silty sand | 2.09-2.09 | 1908.1-2022.6 | 0.89-1.19 | 383.6-531.4 | |

### 3.2.2.2. Modelling assumptions

The point source model has been calculated for point-source equivalent ECFs of 0.5 % and 1.0 % based on the source spectrum shown in Figure 22, and the input hammer energy of 1525 kJ. The point source depth has been chosen as half of the

water depth. Identical environments have been used for both the point source and line source modelling.

#### 3.2.2.3. Results

Figure 30 shows the modelled per-pulse SEL 2 m from the seafloor against distance from the centre of the pile for the PDSM and point source results, along with the measurements made. Figure 31 shows the equivalent depth-averaged results against distance.

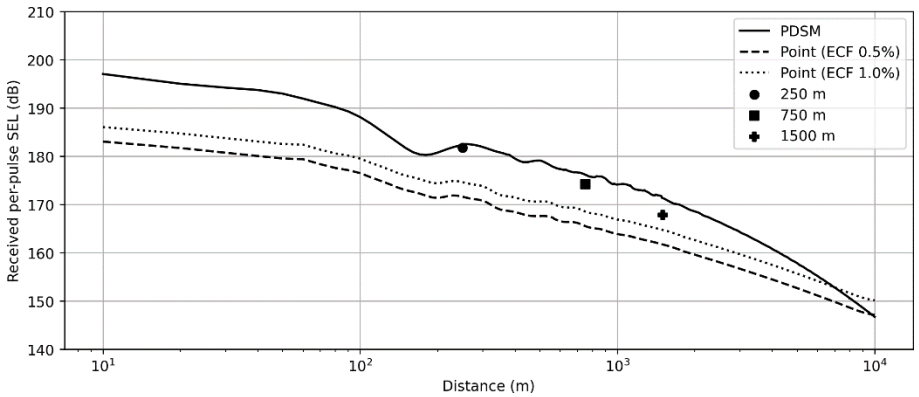


Figure 30. Modelled per-pulse SEL at 2 m above the seafloor for the point-source equivalent ECF models and the line-source model, against the measured results.

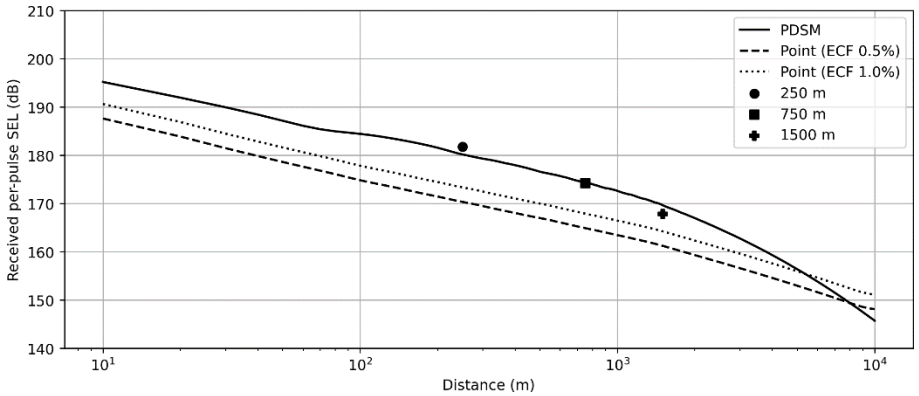


Figure 31. Modelled depth-averaged per-pulse SEL for the point-source equivalent ECF models and the line-source model, against the measured results 2 m from the seabed.

As seen in the previous study, the point-source equivalent ECF model is a poor predictor of sound levels from impact piling. In this case, the sound levels at the receiver locations were underestimated by between 3.3 dB (1500 m receiver, $\beta$ = 1.0 %) and 10.2 dB (250 m receiver, $\beta$ = 0.5 %).

## 3.3. Consideration of Pin Piles

The examples shown in the previous sections principally consider the driving of monopiles. As more wind farms are built in deeper locations there is increased need for the installation of jacket structures. In construction, the jacket structure is deployed on the seabed and secured using a post-piling approach. This involves inserting piles into the skirt sleeves and driving the piles to secure the foundation. Figure 32 shows a drawing of the two foundations.

One key difference between the monopile and jacket pile installations is that in the case of the monopile the pile spans the entire water column at all points in the driving operation, whereas for the jacket pile the wetted length of the pile reduces over the piling sequence. In terms of radiated sound, the same acoustic mechanisms occur in that the stress wave travels down and up the pile producing wavefronts that propagate at the distinctive Mach angle. The reduction of the radiating area in water of the pin pile results in a reduction in radiated sound presuming all other parameters, such as the hammer energy, remain constant.

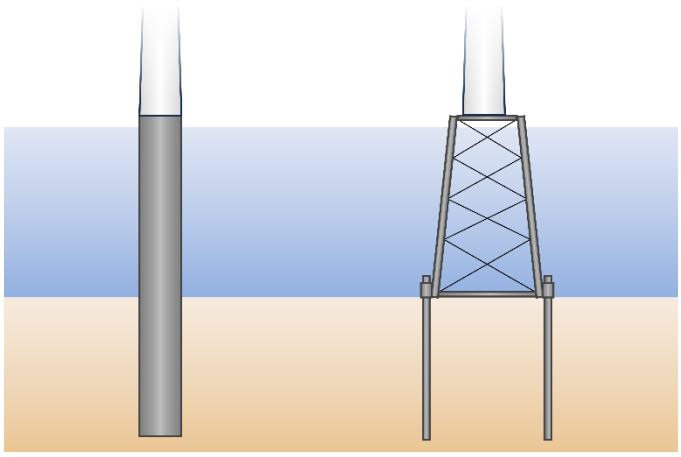

Figure 32. Drawing of monopile foundation (left) and jacket foundation with pin piles (right).

The point at which the radiated sound energy is a maximum, therefore, is determined by the combination of the hammer energy and the remaining stick-up length of the pile. The effect of the stick-up length on the radiated sound from the impacted submerged pile was studied by Lippert et al. (2017). It was found that, for the piles in question (2.44 m outer diameter, 82 m length, 40 m water depth), the change in SEL due to a change in wetted pile length could be calculated as 2.5 dB per 50% reduction in the remaining length of pile above the seabed. Consequently, when considering the worst-case assessment, it is most likely to occur at a point where there is a substantial portion of the pile still in the water column which may not correspond to the maximum hammer energy.

At points where there is little exposed pile in the water column, the propagation is unlikely to follow that of the DCS model. As stated, however, most interest will be at

points where there is still much of the pile in the water column due to the associated higher sound levels. At these points, it is still necessary to consider the pile to be a line source generating wave fronts at the Mach angle rather than a point source.

## 3.4. Sound Propagation Summary

It has been shown in scientific literature that the nature of the propagation of sound from an impacted pile is substantially different from that for a point source. The sound field from the pile constitutes conical wavefronts known as the Mach cone, the angle of which is dictated by the relative sound speed of the water and down the pile. Point monopole sources, conversely, have multiple regimes of propagation initially comprising wavefronts in spherical shells, before transitioning to a cylindrical spreading regime some distance away, with a transition to a mode-stripping region beyond that.

This section provided an investigation into potential differences between generated sound fields based on the propagation assumptions. Examples were shown using geometric models, that take into account the general characteristics of the different propagation regimes, and numerical models, that fully account for the environment and the detailed propagation of the sound wave through the water and sediment.

In the case of the geometric models, results for a single point source were compared to the DCS model. It has been noted that the DCS model provides calculations of transmission loss rather than propagation loss; consequently, it requires a point of reference of another received sound level to generate the sound level as a function of range. Also, whilst the geometric monopole source results clearly show the transition between regions, the transitions are less clear for real environments and more complex source functions.

In the first two geometric examples shown (Figures 9 and 10), the sound levels between the two models were matched at 100 m for a favourable choice of parameters. As this corresponded to the cylindrical spreading regime in the monopole model, the two curves had a reasonable fit over much of the ranges of interest. Where deeper water was considered, there is a greater distance between successive bounces in the DCS model. Consequently, the absorption term takes longer before it starts to dominate, such that the propagation appears cylindrical over longer ranges. In the point source model, the water depth dictates the points at which the spreading regime changes; deeper waters result in an increased distance before propagation changes from spherical to cylindrical.

In the unfavourable case (Figure 11), absorption losses in the DCS model became substantial earlier due to the shallower water. Here, the transmission loss curves were matched at 2 km; however, the two types of propagation resulted in large level differences at ranges from 10 to 1000 m. In the cases of deriving sound levels, although the transmission loss curves can often be made to match for a certain distance, the rate of transmission loss diverges both close to the source and at

greater distances where the absorption term in the DCS model starts to influence the result. At large enough distances, the point source model will always underpredict the transmission loss.

Two numerical examples were provided which are representative of typical modelling for impact assessments. In both cases, sound field levels generated by the point source models differed greatly from those of the line source model. The numerical model matched the general fit of the DCS model and provided a better match against measurements for a benchmarking study. Comparisons were shown against examples of the point-source equivalent ECF model. In these cases, using conversion factors of 0.5 % and 1.0 % underpredicted the sound levels within a few kilometres from the source. Although not shown, it's clear that using a higher conversion factor (i.e., 4 %) would bring sound levels closer to the line source prediction nearer the source; at large distances, however, this would result in increasing overprediction of sound levels, and therefore an overestimate of distances to sound level isopleths.

# 4. Options For Sound Predictions

We have seen from previous sections that predicting radiated sound fields resulting from piling operations is not a straightforward task. There are, however, methods developed and being developed to further improve the sound level forecasts. These vary in complexity and in their range of applications with one comprehensive overview being provided by Tsouvalas (2020). A few approaches for sound level predictions are discussed further here.

## 4.1. Predictions from Existing Measurements

Due to the complexities in modelling sound levels from piling operations, there have been efforts directed into making simpler predictions possible whilst retaining a reasonable level of accuracy. One such effort involves the idea of using scaling factors. The general idea is that, if one has measurements of a piling operation, one can then use these measurements along with calculated adjustments to predict sound fields for the new scenario. The calculated adjustments arise from inputs including a change in the hammer, a change in the pile, or a change in the environment. Consequently, the value of the ECF, as considered in this report, essentially acts as the culmination of these scaling factors that affect the sound levels in the modelled domain.

There has been previous discussion regarding the use of 1.0 % or 0.5 % as an energy conversion factor. As shown in Section 2.1.2, however, calculated values of the ECF vary considerably. It should also be noted that calculations of the point-source equivalent ECF would have been performed using point source models which, as shown in Section 3, are strongly dependent on the measurement location and highly likely to yield an incorrect answer.

It is stressed that the concept of using the ECF is not flawed in itself. However, a single off-the-shelf value cannot capture the separate influences of the hammer properties, the pile properties, and the environment insomuch as how they affect the source level. If an energy conversion approach is to be used, it should be known how the different parameters affect the ECF, and by how much.

### 4.1.1. Scaling laws for unmitigated pile driving

The study, “Scaling laws for unmitigated pile driving: Dependence of underwater noise on strike energy, pile diameter. ram weight, and water depth” by von Pein et al. (2022) involved analysing the effect of changes in the mentioned aspects and the effect each had on the radiated noise. These parameters, the authors believed, would be the main influencers over the radiated noise.

The authors identify the limits of the method and recommend that they are most suitable for distances close to the pile stating that beyond 5 km the influence of

frequency-dependent losses would require further attention. The effect of sediment changes was not investigated due to not being able to generalise soil effects in a simple scaling law. The analyses presented consider the sediment to be an infinite half-space, and as such any sub-bottom reflections and upward refraction effects are not considered. Finally, the study investigated only unmitigated piling operations at this stage.

In terms of hammer energy, it was found that assuming a linear dependence of acoustical energy on the strike energy agrees well with modelled results and reasonably well with measurements. This is in accordance with Figure 1, and also represented in Equation 1 presuming that $\beta$ is independent of the hammer energy.

The effect of the pile diameter has been investigated previously with research by Nehls et al. (2007) suggesting that for a given blow energy, pile diameter alone does not necessarily lead to a change in noise output. The reasoning was that whilst there exists a larger surface area, for a constant energy, the amplitude would reduce. The von Pein report also highlights the ‘interplay’ of numerous factors affected by a change on the diameter on the radiated sound. For a rod, the radial expansion increases linearly with the radius presuming the stress remains the same. To maintain a constant stress in the larger diameter pile, however, the energy must also increase.

One important aspect of the diameter increase is a reduction in the pile ring frequency, $f_{\mathrm{r}}$. It has been shown that if one considers that frequency content of the input energy from the hammer, energy between $0.5\ f_{\mathrm{r}}$ and $0.8\ f_{\mathrm{r}}$ is amplified and more efficiently converted into sound pressure waves than that above the ring frequency (Tsouvalas 2020). Consequently, the excitation force should be considered when determining the effect of a change in pile diameter.

The influence of the ram mass is that it directly affects the initial hammer velocity. The impact velocity, $v_0$, of the ram is $v_0 = \sqrt{2E_{\mathrm{k}}/m_{\mathrm{r}}}$ where $E_{\mathrm{k}}$ is the kinetic energy, and $m_{\mathrm{r}}$ is the ram mass. Consequently, for a fixed hammer energy, an increase in ram mass results in a reduction of impact velocity. The reduction in impact velocity in turn leads to a reduction in the radiated sound. It is noted that the analysis presented in the paper excludes possible influences from changes in hammer element stiffnesses or dimensions, as these factors cannot be easily generalised.

Finally, the effect of a change in water depth is investigated based on transmission losses calculated using the DCS model. The result is that greater water depths result in fewer bottom reflections over a given distance, and thus produces increased sound levels.

It was found that using results from impact piling at 21 wind farms, the SEL at 750 m could be predicted to within -2.3 to +4.2 dB based on the scaling law formulations generated in the project. Deviations were believed to be caused by sediment parameters, interplay between the hammer and monopile combinations, weather and measurement conditions, and possible coupling effect, e.g., with jacket structures.

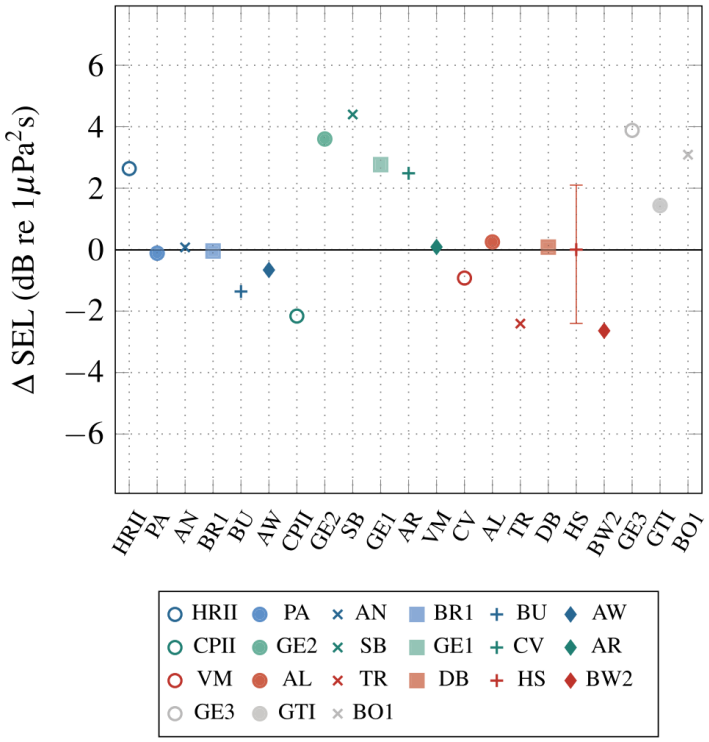


Figure 33. The difference between the measured and scaled results of the SEL at 750 m for all analysed piling locations, scaled with the parameters from piling at Hornsea (HS). Five similar piles were installed at Hornsea providing the range of results. Reproduced from von Pein et al. (2022).

In conclusion, the authors recommend that scaling should either be undertaken over a small number of very similar piling situations or averaged over a large data set. Remaining errors are likely to be down to multiple hammer, pile, and environmental parameters that do not reduce simply to a single scaling factor. The aim of the project, however, was to develop a general tool to allow the calculation of general trends and first estimations.

### 4.1.2. Parametric Analysis and Sensitivity Study

Another approach to pile predictions is provided by the report “A Parametric Analysis and Sensitivity Study of the Acoustic Propagation for Renewable Energy” by Heaney et al. (2020). For this project, the aims were to investigate the sensitivity of the sound levels from piling based on numerous factors, and to provide guidance for future projects as to whether sound levels from new piling operations could be reasonably predicted based an existing set of results or whether results should be generated from new model runs.

Two sites off the United States Atlantic coast were selected for the sensitivity study: Rhode Island and Virginia Beach. The study considered a fixed pile size and hammer, and investigated how changes in the environment affected the radiated sound. The biggest effect on the sound levels was the selection of site, with site selection being a

proxy not only for water depth at the source, but bathymetry across the surrounding region. For this, the differences in SEL were up to 40 dB beyond 20 km from the sites. The next largest influence on radiated sound was the sediment type; as harder sediments reflected more of the energy back into the water column, the sound propagated further than for softer sediment environments. Finally, it was found that the sound speed profile (SSP) had the smallest effect, with better propagation in the winter than in the summer; the warming of the sea surface in summer led to increased refraction towards the seafloor, resulting in more bottom bounces and greater losses.

The authors highlight that there are limiting factors to the use of the results of the study. Firstly, only a single type of pile and input energy was used across the study; the observation is that for different sizes of piles that the noise field will be different and would require new measurements or modelling. Secondly, only vertical piles were considered in this study, and that the sound field from raked piles would have strong azimuthal dependence.

The report recommendations regarding whether existing results could be applied to new results are summarised below:

- Sites that differ in water depth by 50 % should be modelled separately (e.g., water depths of 5, 7, 11, 16, 23, 34, 50 m); results can be interpolated between depths where available.
- Sites where the mean grain size differs by 1 φ or more should be modelled separately.
- Sites run for a different target month should be modelled separately to adequately capture the most likely SSP.
- Sites that differ in distance from the shore by 15 km should be modelled separately.
- Sites that use a different hammer or pile should be modelled separately.

## 4.2. Numerical Modelling

Numerical modelling allows for predictions of the piling noise with reasonable accuracy proving the model inputs and the method of propagation are appropriate. There are numerous advantages to using numerical modelling over the scaling approach in the previous section. There is no requirement for a reference sound level to be used, allowing forecasts to take place in new environments using new pile geometries and hammers. The use of numerical modelling allows for greater control over environmental inputs such as range-varying bathymetry and layered sediments. Additionally, the models are able to take the subterranean sound into account, are effective for propagation into deeper water, and can generate predictions of the sound levels as it varies with depth as well as range.

On top of these benefits, there are additional extended capabilities that can be employed in the modelling to take other situations into account. For example, in the case of underwater piling, more energy emanates from the embedded portion of the pile towards the latter stages of the operation which is harder to reproduce in the scaling or geometric models. Another factor is the use of mitigation strategies to reduce the acoustic impact of larger piles and larger hammers, including pile sleeves and bubble curtains. There are methods developed for numerical models to include such mitigation techniques that are currently beyond the capabilities of the simpler techniques.

Given the nature of piling, the description of the sediment is crucial in both the propagation and source function models for pile driving. In many numerical models, a linearised fluid sediment approximation is used. More recent models, however, have placed greater emphasis on incorporating elastic sediment properties to enhance the accuracy of calculating interface waves and the propagating field within the sediment (Tsouvalas 2020).

The modelling approaches used in numerical methods typically feature a close-range model coupled to a long-range model. The close-range model calculates the acoustic field very close to the pile having taken the pile stress wave into account, while the long-range acoustic model is typically optimised for acoustic propagation.

Numerical modelling of the pile itself is often done using finite-element models, although finite-difference models and semi-analytical models have been used successfully. The purpose of this module is to model the response of the pile to the input force (often derived from separate driveability models, or analytical functions), and how the pile response is manifest in the acoustic wave at the model boundary. This takes into account the progression of the stress wave down the pile with its reflections and the resulting conical wavefront emanating from the pile. The output of the close-range model is used as the input to the long-range model. Common options for the long-range model are described briefly in Section 2.2.1. Whilst there may have been more recent additions, Tsouvalas (2020) provides a list of those impact piling source and propagation models either validated against experimental data or numerical benchmark studies.

# 5. Summary and Recommendations

This section provides a summary of the review contents and the recommendations for the prediction of the underwater sound fields resulting from impact piling.

- The point-source equivalent ECF method comprises:
  - generating a single value broadband ESL for which the inputs are the hammer energy and the point-source equivalent ECF.
  - Calculating a source spectrum using recorded results scaled to the generated ESL.
  - Using a point source propagation model to generate the per-pulse SEL sound fields from which impacts are assessed.
- Benefits of the method include:
  - its simplicity in that it requires only the hammer energy and a value for $\beta$ to generate a source function.
  - the speed at which one can generate source inputs and modelling outputs.
  - its exploitation of a powerful physical principle, i.e., conservation of energy
- Shortcomings of the method exist in the source generation:
  - The ratio of hammer input energy to radiated acoustic energy in the water column is not a fixed universal value. Recorded values range from 0.17 % to 1.56 %, which equates to a range of 9.6 dB.
  - The dependence of this ratio on input parameters based on the pile, the hammer, the environment, and the geometry is not well understood.
- Shortcomings also exist in the modelled propagation:
  - The nature of propagation from point source models is substantially different from one suitable for piling noise. It is also noted that a source level does not exist for a pile, and that it is unhelpful to attempt to characterise it as such.
  - Predictions of distances to sound level thresholds can often be out by orders of magnitude, with examples showing errors up to 10 dB within 5 km of the pile.
- Effects are compounded when both are used:
  - In one reported numerical modelling example, combining the point-source equivalent ECF generated point source using $\beta$ = 0.5 % with the point source propagation model yielded underestimates of the per-pulse SEL of between 9.5 and 12.1 dB between 100 and 1000 m from the pile when compared against the dedicated pile model.

The following recommendations are made:

- Modelling using the point-source equivalent ECF method described above should not be used, having been entirely superseded by more modern approaches and shown to be inaccurate for sound field predictions.
- Numerical modelling provides the greatest flexibility in terms of selection of hammer, pile, and environment and is considered the leading method, provided:
  - The Mach wave nature of piling is taken into account in the source modelling, and
  - This is coupled to a propagation model that will support the Mach wave.
- Genuine values of the ECF, however, could be used for sound level predictions provided they are used with a model that supports them, e.g., DCS model.
- If a measurement or measurements exist for the scenario in question, the DCS model can be used to predict sound levels at other distances up to approximately 5 km using the reference sound level.
- Where measurements exist of similar scenarios, these may be used with adjustments to apply to alternative scenarios with caution.
  - Possibilities include change in hammer energy, change in ram mass, change in pile diameter, and change in water depth.
  - The difficulty of this approach is knowing how to determine whether changes are too numerous or great. If in doubt, it is recommended to remodel using numerical techniques.

## Glossary

Unless otherwise stated in an entry, these definitions are consistent with ISO 18405 (2017).

### 1/3-octave

One third of an octave. *Note*: A 1/3-octave is approximately equal to one decidecade (1/3 oct ≈ 1.003 ddec).

### 1/3-octave-band

Frequency band whose bandwidth is one 1/3-octave. *Note*: The bandwidth of a 1/3-octave-band increases with increasing centre frequency.

### absorption

The conversion of sound energy to heat energy. Specifically, the reduction of sound pressure amplitude due to particle motion energy converting to heat in the propagation medium.

### acoustic impedance

The ratio of the sound pressure in a medium to the volume flow rate of the medium through a specified surface due to the sound wave. It is a measure of how well sound propagates through a particular medium.

### attenuation

The gradual loss of acoustic energy from absorption and scattering as sound propagates through a medium. Attenuation depends on frequency—higher frequency sounds are attenuated faster than lower frequency sounds.

### auditory frequency weighting

The process of applying an auditory frequency-weighting function. An example for marine mammals are the auditory frequency-weighting functions published by Southall et al. (2007).

### auditory frequency-weighting function

Frequency-weighting function describing a compensatory approach accounting for a species' (or functional hearing group's) frequency-specific hearing sensitivity.

### azimuth

A horizontal angle relative to a reference direction, which is often magnetic north or the direction of travel. In navigation it is also known as bearing.

### bandwidth

A range within a continuous band of frequencies. Unit: hertz (Hz).

**broadband level**

The total level measured over a specified frequency range. If the frequency range is unspecified, the term refers to the entire measured frequency range.

**compressional wave**

A mechanical vibration wave in which the direction of particle motion is parallel to the direction of propagation. Also called a longitudinal wave. In seismology/geophysics, it's called a primary wave or P-wave. Shear waves in the seabed can be converted to compressional waves in water at the water-seabed interface.

**decade**

Logarithmic frequency interval whose upper bound is ten times larger than its lower bound (ISO 80000-3:2006). For example, one decade up from 1000 Hz is 10,000 Hz, and one decade down is 100 Hz.

**decibel (dB)**

Unit of level used to express the ratio of one value of a power quantity to another on a logarithmic scale. Especially suited to quantify variables with a large dynamic range.

**decidecade**

One tenth of a decade. Approximately equal to one third of an octave (1 ddec ≈ 0.3322 oct), and for this reason sometimes referred to as a 1/3-octave.

**decidecade band**

Frequency band whose bandwidth is one decidecade. *Note*: The bandwidth of a decidecade band increases with increasing centre frequency.

**energy source level**

A property of a sound source equal to the sound exposure level measured in the far field plus the propagation loss from the acoustic centre of the source to the receiver position. Unit: decibel (dB). Reference value: 1 $\mu Pa^2\,m^2\,s$.

**ensonified**

Exposed to sound.

**far field**

The zone where, to an observer, sound originating from an array of sources (or a spatially distributed source) appears to radiate from a single point.

**Fourier transform, Fourier synthesis**

A mathematical technique which, although it has varied applications, is referenced in a physical data acquisition context as a method used in the process of deriving a spectrum estimate from time-series data (or the reverse process, termed the inverse

Fourier transform). A computationally efficient numerical algorithm for computing the Fourier transform is known as the fast Fourier transform (FFT).

### frequency

The rate of oscillation of a periodic function measured in cycles per unit time. The reciprocal of the period. Unit: hertz (Hz). Symbol: *f*. 1 Hz is equal to 1 cycle per second.

### frequency weighting

The process of applying a frequency-weighting function.

### frequency-weighting function

The squared magnitude of the sound pressure transfer function (ISO 18405:2017). For sound of a given frequency, the frequency-weighting function is the ratio of output power to input power of a specified filter, sometimes expressed in decibels. Examples include the following:

- *Auditory frequency-weighting function*: compensatory frequency-weighting function accounting for a species' (or functional hearing group's) frequency-specific hearing sensitivity.
- *System frequency-weighting function*: frequency-weighting function describing the sensitivity of an acoustic recording system, which typically consists of a hydrophone, one or more amplifiers, and an analogue-to-digital converter.

### functional hearing group

Category of animal species when classified according to their hearing sensitivity, hearing anatomy, and susceptibility to sound. For marine mammals, initial groupings were proposed by Southall et al. (2007), and revised groupings are developed as new research/data becomes available. Revised groupings proposed by Southall et al. (2019) include low-frequency cetaceans, high-frequency cetaceans, very high-frequency cetaceans, phocid carnivores in water, other carnivores in water, and sirenians. See auditory frequency-weighting functions, which are often applied to these groups. Example hearing groups for fish include species for which the swim bladder is involved in hearing, species for which the swim bladder is not involved in hearing, and species without a swim bladder (Popper et al. 2014).

### geoacoustic

Relating to the acoustic properties of the seabed.

### harmonic

A sinusoidal sound component that has a frequency that is an integer multiple of the frequency of a sound to which it is related. For a sound with a fundamental frequency of *f*, the harmonics have frequencies of 2*f*, 3*f*, 4*f*, etc.

**hertz (Hz)**

Unit of frequency defined as one cycle per second. Often expressed in multiples such as kilohertz (1 kHz = 1000 Hz).

**hydrophone**

An underwater sound pressure transducer. A passive electronic device for recording or listening to underwater sound.

**impulsive sound**

Qualitative term meaning sounds that are typically transient, brief (less than 1 s), broadband, with rapid rise time and rapid decay. They can occur in repetition or as a single event. Sources of impulsive sound include, among others, explosives, seismic airguns, and impact pile drivers.

**isopleth**

A line drawn on a map through all points having the same value of some specified quantity (e.g., sound pressure level isopleth).

**level**

A measure of a quantity expressed as the logarithm of the ratio of the quantity to a specified reference value of that quantity. For example, a value of sound pressure level with reference to 1 $\mu Pa^2$ can be written in the form *x* dB re 1 $\mu Pa^2$.

**monopole source level (MSL)**

A source level that has been calculated using an acoustic model that accounts for the effect of the sea-surface and seabed on sound propagation, assuming a point source (monopole). Often used to quantify source levels of vessels or industrial operations from measurements. See also radiated noise level.

**octave**

The interval between a sound and another sound with double or half the frequency. For example, one octave above 200 Hz is 400 Hz, and one octave below 200 Hz is 100 Hz.

**parabolic equation method**

A computationally efficient solution to the acoustic wave equation that is used to model propagation loss. The parabolic equation approximation omits effects of backscattered sound (which are negligible for most ocean-acoustic propagation problems), simplifying the computation of propagation loss.

### peak sound pressure level (PK), zero-to-peak sound pressure level

The level ($L_{pk}$) of the squared maximum magnitude of the sound pressure ($p_{pk}^2$) in a stated frequency band and time window. Defined as $L_{pk} = 10\log_{10}(p_{pk}^2/p_0^2) = 20\log_{10}(p_{pk}/p_0)$. Unit: decibel (dB). Reference value ($p_0^2$) for sound in water: 1 μPa².

### peak-to-peak sound pressure

The difference between the maximum and minimum sound pressure over a specified frequency band and time window. Unit: pascal (Pa).

### permanent threshold shift (PTS)

An irreversible loss of hearing sensitivity caused by excessive noise exposure. Considered auditory injury. Compare with temporary threshold shift.

### point source

A source that radiates sound as if from a single point.

### propagation loss (PL)

Difference between a source level (SL) and the level at a specified location, PL($x$) = SL − $L$($x$). Unit: decibel (dB). See also transmission loss.

### radiated noise level (RNL)

A source level that has been calculated assuming sound pressure decays geometrically with distance from the source, with no influence of the sea-surface or seabed. Often used to quantify source levels of vessels or industrial operations from measurements. See also monopole source level.

### received level

The level of a given field variable measured (or that would be measured) at a given location. reference value

Standard value of a quantity used for calculating underwater sound level. The reference value depends on the quantity for which the level is being calculated:

| Quantity | Reference value |
|---|---|
| Sound pressure | $p_0^2$ = 1 μPa² or $p_0$ = 1 μPa |
| Sound exposure | $E_0$ = 1 μPa² s |
| Sound particle displacement | $\delta_0^2$ = 1 pm² |
| Sound particle velocity | $u_0^2$ = 1 nm²/s² |
| Sound particle acceleration | $a_0^2$ = 1 μm²/s⁴ |

**shear wave**

A mechanical vibration wave in which the direction of particle motion is perpendicular to the direction of propagation. Also called a secondary wave or S-wave. Shear waves propagate only in solid media, such as sediments or rock. Shear waves in the seabed can be converted to compressional waves in water at the water-seabed interface.

**sound**

A time-varying disturbance in the pressure, stress, or material displacement of a medium propagated by local compression and expansion of the medium. In common meaning, a form of energy that propagates through media (e.g., water, air, ground) as pressure waves.

**sound exposure**

Time integral of squared sound pressure over a stated time interval in a stated frequency band. The time interval can be a specified time duration (e.g., 24 h) or from start to end of a specified event (e.g., a pile strike, an airgun pulse, a construction operation). Unit: pascal squared second ($Pa^2\,s$). Symbol: $E$.

**sound exposure level (SEL)**

The level ($L_E$) of the sound exposure ($E$) in a stated frequency band and time window: $L_E = 10\log_{10}(E/E_0)$ (ISO 18405:2017). Unit: decibel (dB). Reference value ($E_0$) for sound in water: 1 $\mu Pa^2\,s$.

**sound field**

Region containing sound waves.

**sound intensity**

Product of the sound pressure and the sound particle velocity (ISO 18405:2017). The magnitude of the sound intensity is the sound energy flowing through a unit area perpendicular to the direction of propagation per unit time. Unit: watt per metre squared ($W/m^2$). Symbol: $I$.

**sound particle velocity**

The velocity of a particle in a material moving back and forth in the direction of the pressure wave. Unit: meter per second (m/s). Symbol: $u$.

**sound pressure**

The contribution to total pressure caused by the action of sound (ISO 18405:2017). Unit: pascal (Pa). Symbol: $p$.

### sound pressure level (SPL), rms sound pressure level

The level ($L_p$) of the time-mean-square sound pressure ($p^2_{\mathrm{rms}}$) in a stated frequency band and time window: $L_p = 10\log_{10}(p^2_{\mathrm{rms}}/p^2_0) = 20\log_{10}(p_{rms}/p_0)$, where rms is the abbreviation for root-mean-square. Unit: decibel (dB). Reference value ($p^2_0$) for sound in water: 1 μPa$^2$. SPL can also be expressed in terms of the root-mean-square (rms) with a reference value of $p_0$ = 1 μPa. The two definitions are equivalent.

### sound speed profile (SSP)

The speed of sound in the water column as a function of depth below the water surface.

### source level (SL)

A property of a sound source equal to the sound pressure level measured in the far field plus the propagation loss from the acoustic centre of the source to the receiver position. Unit: decibel (dB). Reference value: 1 μPa$^2$ m$^2$.

### temporary threshold shift (TTS)

Reversible loss of hearing sensitivity caused by noise exposure. Compare with permanent threshold shift.

### transmission loss (TL)

The difference between a specified level at one location and that at a different location: $\mathrm{TL}(x_1,x_2) = L(x_1) - L(x_2)$ (ISO 18405:2017). Unit: decibel (dB). See also propagation loss.

### unweighted

Term indicating that no frequency-weighting function is applied.

### wavelength

Distance over which a wave completes one cycle of oscillation. Unit: metre (m). Symbol: λ.

## Literature Cited

[CEFAS] Centre for Environment, Fisheries and Aquaculture Science. 2018a. *Moray West Offshore Windfarm. Technical Appendix 9.2: Underwater Noise Modelling*. https://www.moraywest.com/download_file/force/650/219.

[CEFAS] Centre for Environment, Fisheries and Aquaculture Science. 2018b. *Inch Cape Offshore Environmental Impact Assessment: Appendix 9B Underwater Noise Modelling*. https://www.inchcapewind.com/wp-content/uploads/2020/10/IC01-EC-OFA-002-090-RRP-APE-002_Appendix_9B_Underwater_Noise_Modelling_REV_B.pdf.

[CEFAS] Centre for Environment, Fisheries and Aquaculture Science. 2018c. *Inch Cape Offshore Environmental Impact Assessment: Appendix 10B Underwater Noise Modelling Using a 1 % Conversion Factor*. https://www.inchcapewind.com/wp-content/uploads/2020/10/IC01-EC-OFA-002-100-RRP-APE-002_Appendix_10B_Under_Water_Noise_Modelling_Using_a_1_..._RevA.pdf.

[CEFAS] Centre for Environment, Fisheries and Aquaculture Science. 2018d. Seagreen EIA Report Vol 3 App 10E Piling Noise Impact Assessment using A 1% Acoustic Energy Conversion Factor and use of Acoustic Deterrent Devices. https://www.seagreenwindenergy.com/_files/ugd/fe5128_15df6126e6b44b108600d1edfcdedab0.pdf.

[CEFAS] Centre for Environment, Fisheries and Aquaculture Science. 2019. *Moray East Offshore Wind Farm: Wind Farm Piling Strategy Appendix 1 Underwater Noise Modelling*. https://marine.gov.scot/sites/default/files/moray_east_wind_farm_ps_v.3_redacted.pdf.

[ISO] International Organization for Standardization. 2006. *ISO 80000-3:2006 Quantities and units – Part 3: Space and time*. https://www.iso.org/standard/31888.html.

[ISO] International Organization for Standardization. 2017. *ISO 18405:2017. Underwater acoustics – Terminology*. Geneva. https://www.iso.org/standard/62406.html.

[Seiche Ltd]. 2022. *Berwick Bank Wind Farm Digital Consent Application / EIA Documents. Volume 3 Appendix 10.1 Subsea Noise Technical Report* (webpage). https://berwickbank-eia.com/offshore-eia/vol3-ap1001-Subsea-Noise-Technical-Report/. (Accessed 30th March).

Ainslie, M.A. 2010. *Principles of Sonar Performance Modeling*. Praxis Books. Springer, Berlin. https://doi.org/10.1007/978-3-540-87662-5.

Ainslie, M.A., P.H. Dahl, C.A.F. de Jong, and R.M. Laws. 2014. *Practical Spreading Laws: The Snakes and Ladders of Shallow Water Acoustics*. *UA2014 - 2nd International Conference and Exhibition on Underwater Acoustics*, 22-27 Jun 2014, Island of Rhodes, Greece, pp. 879-886.

Ainslie, M.A., M.B. Halvorsen, R.A.J. Müller, and T. Lippert. 2020. Application of damped cylindrical spreading to assess range to injury threshold for fishes from impact pile driving. *Journal of the Acoustical Society of America* 148(1): 108-121. https://doi.org/10.1121/10.0001443.

Buckingham, M.J. 2005. Compressional and shear wave properties of marine sediments: Comparisons between theory and data. *Journal of the Acoustical Society of America* 117: 137-152. https://doi.org/10.1121/1.1810231.

Collins, M.D. 1993. A split-step Padé solution for the parabolic equation method. *Journal of the Acoustical Society of America* 93(4): 1736-1742. https://doi.org/10.1121/1.406739.

Dahl, P.H., P.G. Reinhall, and D.M. Farrell. 2012. *Transmission loss and range, depth scales associated with impact pile driving*. *Processings of the 11th European Conference on Underwater Acoustics*. Institute of Acoustics, Edinburgh, UK, pp. 1860-1867.

Dahl, P.H. and P.G. Reinhall. 2013. Beam forming of the underwater sound field from impact pile driving. *Journal of the Acoustical Society of America* 134(1): EL1-EL6. https://doi.org/10.1121/1.4807430.

Dahl, P.H., C.A.F. de Jong, and A.N. Popper. 2015. The Underwater Sound Field from Impact Pile Driving and Its Potential Effects on Marine Life. *Acoustics Today* 11(2): 18-25. https://acousticstoday.org/issues/2015AT/Spring2015/#?page=20.

Dahl, P.H. and D.R. Dall'Osto. 2017. On the underwater sound field from impact pile driving: Arrival structure, precursor arrivals, and energy streamlines. *Journal of the Acoustical Society of America* 142(2): 1141-1155. https://doi.org/10.1121/1.4999060.

de Jong, C.A.F. and M.A. Ainslie. 2008. Underwater radiated noise due to the piling for the Q7 Offshore Wind Park. *Journal of the Acoustical Society of America* 123(5): 2987. https://doi.org/10.1121/1.2932518.

de Jong, C.A.F., B. Binnerts, M.K. Prior, M. Colin, M.A. Ainslie, I. Mulder, and I. Hartstra. 2019. *Wozep–WP2: Update of the Aquarius models for marine pile driving sound predictions*. Report by TNO. Document Number R11671. 94 p.

Etter, P.C. 2012. Advanced Applications for Underwater Acoustic Modeling. *Advances in Acoustics and Vibration* 2012: 1-28.

Farcas, A., P.M. Thompson, and N.D. Merchant. 2016. Underwater noise modelling for environmental impact assessment. *Environmental Impact Assessment Review* 57: 114-122. https://doi.org/10.1016/j.eiar.2015.11.012.

Farcas, A., N.D. Merchant, and R.C. Faulkner. 2018. *Seagreen EIA Report Vol 3 App 10B CEFAS Noise Modelling Technical Report*. Cefas. https://www.seagreenwindenergy.com/_files/ugd/fe5128_180f558f760f404bb1dc9b4fa99254ab.pdf.

Faulkner, R.C., A. Farcas, M. Nimak-Wood, and H. Buckley. 2021. *Underwater noise effect assessment for the Sizewell C revised marine freight options*. The Sizewell C Project. https://infrastructure.planninginspectorate.gov.uk/wp-content/ipc/uploads/projects/EN010012/EN010012-006230-Sizewell%20C%20Project%20-%20Other-%20Underwater%20Noise%20Report.pdf.

Graham, I.M., N.D. Merchant, A. Farcas, T.R. Barton, B. Cheney, S. Bono, and P.M. Thompson. 2019. Harbour porpoise responses to pile-driving diminish over time. *Royal Society Open Science* 6(6): 190335. https://doi.org/10.1098/rsos.190335.

Hamilton, E.L. 1980. Geoacoustic modeling of the sea floor. *Journal of the Acoustical Society of America* 68(5): 1313-1340. https://doi.org/10.1121/1.385100.

Harrison, C.H. and J.A. Harrison. 1995. A simple relationship between frequency and range averages for broadband sonar. *Journal of the Acoustical Society of America* 97(2): 1314-1317. https://doi.org/10.1121/1.412172.

Harrison, C.H. 2013. Ray convergence in a flux-like propagation formulation. *J Acoust Soc Am* 133(6): 3777-89. NLM. https://www.ncbi.nlm.nih.gov/pubmed/23742332.

Heaney, K.D., M.A. Ainslie, M.B. Halvorsen, K.D. Seger, R.A.J. Müller, M.J.J. Nijhof, and T. Lippert. 2020. *A Parametric Analysis and Sensitivity Study of the Acoustic Propagation for Renewable Energy Sources*. Report by CSA Ocean Sciences Inc. for US Department of the Interior, Bureau of Ocean Energy Management, Office of Renewable Energy Programs. OCS Study BOEM 2020-011, Sterling, VA. 165 p. https://espis.boem.gov/final%20reports/BOEM_2020-011.pdf.

Holzer, T.L., M.J. Bennett, T.E. Noce, and J.C. Tinsley. 2005. Shear-Wave Velocity of Surficial Geologic Sediments in Northern California: Statistical Distributions and Depth Dependence. *Earthquake Spectra* 21(1): 161-177. https://doi.org/10.1193/1.1852561.

Jensen, F.B., W.A. Kuperman, M.B. Porter, and H. Schmidt. 2011. *Computational Ocean Acoustics*. 2nd edition. AIP Series in Modern Acoustics and Signal Processing. AIP Press - Springer, New York. 794 p. https://doi.org/10.1007/978-1-4419-8678-8.

Lippert, S., M. Huisman, M. Ruhnau, O. von Estorff, and K. van Zanwijk. 2017. *Prognosis of underwater pile driving noise for submerged skirt piles of jacket structures*. *4th Underwater Acoustics Conference and Exhibition (UACE 2017)*, 2-8 Sep 2017, Skiathos, Greece. https://www.uaconferences.org/docs/UACE2017_Papers/903_UACE2017.pdf.

Lippert, T., M. Galindo-Romero, A.N. Gavrilov, and O. von Estorff. 2015. Empirical estimation of peak pressure level from sound exposure level. Part II: Offshore impact pile driving noise. *Journal of the Acoustical Society of America* 138(3): EL287-EL292. https://doi.org/10.1121/1.4929742.

Lippert, T., M.A. Ainslie, and O. von Estorff. 2018. Pile driving acoustics made simple: Damped cylindrical spreading model. *Journal of the Acoustical Society of America* 143(1): 310-317. https://doi.org/10.1121/1.5011158.

MacGillivray, A.O. 2014. A model for underwater sound levels generated by marine impact pile driving. *Proceedings of Meetings on Acoustics* 20(1). https://doi.org/10.1121/2.0000030

Nehls, G., K. Betke, S. Eckelmann, and M. Ros. 2007. *Assessment and costs of potential engineering solutions for the mitigation of the impacts of underwater noise arising from the construction of offshore windfarms*. Document Number Report by BioConsult SH for COWRIE.

Pile Dynamics, Inc. 2010. GRLWEAP. https://www.pile.com/.

Popper, A.N., A.D. Hawkins, R.R. Fay, D.A. Mann, S. Bartol, T.J. Carlson, S. Coombs, W.T. Ellison, R.L. Gentry, et al. 2014. *Sound Exposure Guidelines for Fishes and Sea Turtles: A Technical Report prepared by ANSI-Accredited Standards Committee S3/SC1 and registered with ANSI*. ASA S3/SC1.4 TR-2014. SpringerBriefs in Oceanography. ASA Press and Springer. https://doi.org/10.1007/978-3-319-06659-2.

Reinhall, P.G. and P.H. Dahl. 2011. Underwater Mach wave radiation from impact pile driving: Theory and observation. *Journal of the Acoustical Society of America* 130(3): 1209-1216. https://doi.org/10.1121/1.3075600.

Robinson, S.P., P.A. Lepper, and J. Ablitt. 2007. The measurement of the underwater radiated noise from marine piling including characterisation of a" soft start" period. *OCEANS 2007*. 18-21 Jun 2007. IEEE, Aberdeen, UK. pp. 732-737. https://doi.org/10.1109/OCEANSE.2007.4302326.

RPS, G.C. Ltd, and B.a.M. Marine. 2015. *Beatrice Offshore Wind Farm Piling Strategy*. Document Number LF000005-PLN-142. https://marine.gov.scot/sites/default/files/00522494.pdf.

Sertlek, H.Ö. and M.A. Ainslie. 2014. A depth-dependent formula for shallow water propagation. *Journal of the Acoustical Society of America* 136(2): 573-582. https://doi.org/10.1121/1.4884762.

Sertlek, H.Ö., M.A. Ainslie, and K.D. Heaney. 2019. Analytical and Numerical Propagation Loss Predictions for Gradually Range-Dependent Isospeed Waveguides. *IEEE Journal of Oceanic Engineering* 44(4): 1240-1252. https://doi.org/10.1109/JOE.2018.2865640.

Southall, B.L., A.E. Bowles, W.T. Ellison, J.J. Finneran, R.L. Gentry, C.R. Greene, Jr., D. Kastak, D.R. Ketten, J.H. Miller, et al. 2007. Marine Mammal Noise Exposure Criteria: Initial Scientific Recommendations. *Aquatic Mammals* 33(4): 411-521. https://doi.org/10.1578/AM.33.4.2007.411.

Southall, B.L., J.J. Finneran, C.J. Reichmuth, P.E. Nachtigall, D.R. Ketten, A.E. Bowles, W.T. Ellison, D.P. Nowacek, and P.L. Tyack. 2019. Marine Mammal Noise Exposure Criteria: Updated Scientific Recommendations for Residual Hearing Effects. *Aquatic Mammals* 45(2): 125-232. https://doi.org/10.1578/AM.45.2.2019.125.

Thompson, P.M., I.M. Graham, B. Cheney, T.R. Barton, A. Farcas, and N.D. Merchant. 2020. Balancing risks of injury and disturbance to marine mammals when pile driving at offshore windfarms. *Ecological Solutions and Evidence* 1(2).

Tsouvalas, A. 2020. Underwater Noise Emission Due to Offshore Pile Installation: A Review. *Energies* 13(12): 3037. https://doi.org/10.3390/en13123037.

von Pein, J., T. Lippert, S. Lippert, and O. von Estorff. 2022. Scaling laws for unmitigated pile driving: Dependence of underwater noise on strike energy, pile diameter, ram weight, and water depth. *Applied Acoustics* 198: 108986. https://doi.org/10.1016/j.apacoust.2022.108986.

Wang, L., K.D. Heaney, T. Pangerc, P. Theobald, S. Robinson, and M.A. Ainslie. 2014. *Review of underwater acoustic propagation models*. Document Number AC 12 Report Number 1754-2936. Report by National Physical Laboratory, OASIS, and TNO.

Weston, D.E. 1976. Propagation in water with uniform sound velocity but variable-depth lossy bottom. *Journal of Sound and Vibration* 47(4): 473-483. https://doi.org/10.1016/0022-460X(76)90874-9.

Zampolli, M., M.J.J. Nijhof, C.A.F. de Jong, M.A. Ainslie, E.H.W. Jansen, and B.A.J. Quesson. 2013. Validation of finite element computations for the quantitative prediction of underwater noise from impact pile driving. *Journal of the Acoustical Society of America* 133(1): 72-81. https://doi.org/10.1121/1.4768886.

# Appendix A. Pile Driving Source Model

A physical model of pile vibration and near-field sound radiation is used to calculate the radiated sound from impact piling. The physical model employed in this study computes the underwater vibration and sound radiation of a pile by solving the theoretical equations of motion for axial and radial vibrations of a cylindrical shell. These equations of motion are solved subject to boundary conditions, which describe the forcing function of the hammer at the top of the pile and the soil resistance at the base of the pile (Figure A-1). Damping of the pile vibration due to radiation loading is computed for Mach waves emanating from the pile wall. The equations of motion are discretised using the finite difference (FD) method and are solved on a discrete time and depth mesh.

To model the sound emissions from the piles, the force of the pile driving hammers also had to be modelled. The force at the top of each pile was computed using the GRLWEAP 2010 wave equation model (GRLWEAP, Pile Dynamics 2010), which includes a large database of simulated hammers—both impact and vibratory—based on the manufacturers' specifications. The forcing functions from GRLWEAP were used as inputs to the FD model to compute the resulting pile vibrations.

The sound radiating from the pile itself is simulated using a vertical array of discrete point sources. The point sources are centred on the pile axis. Their amplitudes are derived using an inverse technique, such that their collective particle velocity, calculated using a near-field wave-number integration model, matches the particle velocity in the water at the pile wall. The sound field propagating away from the vertical source array is then calculated using a time-domain acoustic propagation model (i.e., RAM). MacGillivray (2014) describes the theory behind the physical model in more detail.

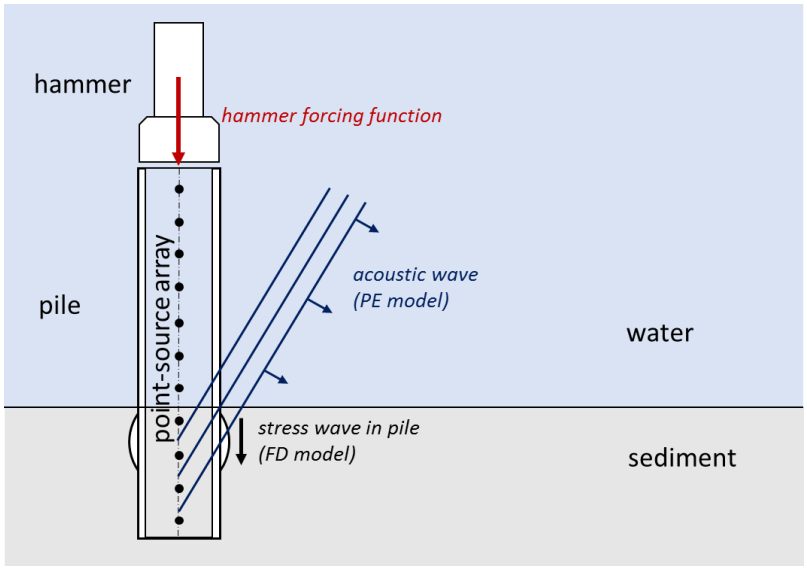


Figure A-1. Physical model geometry for impact driving of a cylindrical pile (vertical cross-section). The hammer forcing function is used with the finite difference (FD) model to compute the stress wave vibration in the pile. A vertical array of point sources is used with the parabolic equation (PE) model to compute the acoustic waves that the pile wall radiates.

This publication is available at **www.gov.scot**

Any enquiries regarding this publication should be sent to us at

The Scottish Government
St Andrew's House
Edinburgh
EH1 3DG

ISBN: 978-1-83521-535-7 (web only)

Published by The Scottish Government, October 2023

Produced for The Scottish Government by APS Group Scotland, 21 Tennant Street, Edinburgh EH6 5NA
PPDAS1377674 (10/23)

**w w w . g o v . s c o t**